Accepted Manuscript

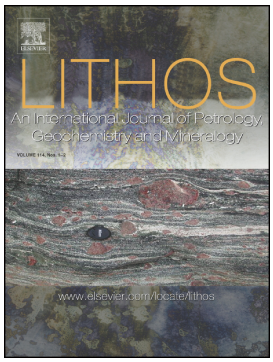

Tectonic control on the genesis of magmas in the New Hebrides arc (Vanuatu)

Christoph Beier, Philipp A. Brandl, Selma M. Lima, Karsten M. Haase

PII: S0024-4937(18)30168-3
DOI: doi:10.1016/j.lithos.2018.05.011
Reference: LITHOS 4657

To appear in:

Received date: 31 January 2018
Accepted date: 10 May 2018

Please cite this article as: Christoph Beier, Philipp A. Brandl, Selma M. Lima, Karsten M. Haase , Tectonic control on the genesis of magmas in the New Hebrides arc (Vanuatu). The address for the corresponding author was captured as affiliation for all authors. Please check if appropriate. Lithos(2018), doi:10.1016/j.lithos.2018.05.011

Tectonic control on the genesis of magmas in the New Hebrides arc (Vanuatu)

Christoph Beier[1], Philipp A. Brandl[2], Selma M. Lima[1] and Karsten M. Haase[1]

[1]GeoZentrum Nordbayern, Friedrich-Alexander Universität Erlangen-Nürnberg, Schlossgarten 5, D-91054 Erlangen, Germany, Email: christoph.beier@fau.de

[2]GEOMAR Helmholtz-Zentrum für Ozeanforschung Kiel, Wischhofstraße 1-3, 24148 Kiel, Germany

ABSTRACT

We present here new bathymetric, petrological and geochemical whole rock, glass and mineral data from the submarine Epi volcano in the New Hebrides (Vanuatu) island arc. The structure has previously been interpreted to be part of a larger caldera structure but new bathymetric data reveal that the volcanic cones are aligned along shear zones controlled by the local tectonic stress field parallel to the recent direction of subduction. We aim to test if there is an interaction between local tectonics and magmatism and to what extent the compositions of island arc volcanoes may be influenced by their tectonic setting. Primitive submarine Epi lavas and those from the neighbouring Lopevi and Ambrym islands originate from a depleted mantle wedge modified by addition of subduction zone components. Incompatible element ratios sensitive to fluid input (e.g., Th/Nb, Ce/Yb) in the lavas are positively correlated with those more sensitive to mantle wedge depletion (e.g., Nb/Yb, Zr/Nb) amongst the arc volcanoes suggesting that fluids or melts from the subducting sediments have a stronger impact on the more depleted compositions of the mantle wedge. The whole rock, glass and mineral major and trace element compositions and the occurrence of exclusively normally zoned clinopyroxene and plagioclase crystals combined with the

absence of inversely zoned crystals and water-bearing phases in both mafic and evolved lavas suggest that the erupted melt was relatively dry compared to other subduction zone melts and has experienced little disequilibrium modification by melt mixing or assimilation. Our data also imply that differentiation of amphibole is not required to explain the incompatible element patterns but may rather result from extensive clinopyroxene fractionation in agreement with petrographic observations. Thermobarometric calculations indicate that the melts fractionated continuously during ascent, contrasting with fractionation during stagnation in an established crustal magma reservoir. We interpret the occurrence of this fractional crystallisation end-member in a relatively thick island arc crust (~30 km thickness) to result from isolated and relatively rapid ascent of melts, most likely through a complex system of dykes and sills that developed due to the tectonic positioning of Epi in a complex tectonic zone between a compressional environment in the north and an extensional setting in the south. We can show that the alignment of the cones largely depends on the local tectonic stress field at Epi that is especially influenced by a large dextral strike-slip zone, indicating that structural features have a significant impact on the location and composition of volcanic edifices.

Keywords: Vanuatu; *New Hebrides*; *silicic melt; island arc; magma evolution; structural control; geodynamics*

- Epi melts have experienced no disequilibrium modification by mixing or assimilation
- Melts fractionate continuously while ascending, rather than stagnating
- Magma ascent is through a complex system of dykes and sills
- Epi situated between compressional and extensional regime on thick island arc crust
- Structural features have impact on focusing and composition of island arc magmas

1. INTRODUCTION

The origin, ascent, and emplacement of silicic melts at convergent margins leads to a chemical differentiation and stratification of the island arc crust (Arculus, 1999; Bachmann and Huber, 2016; Haase et al., 2011; Taylor et al., 1969) that may eventually act as a precursor for the formation of continental crust (Adam et al., 2012; Polat, 2012). Silicic melts in subduction zone settings form either from partial melting of the hydrothermally altered subducting igneous crust (Pertermann and Hirschmann, 2003; Smith et al., 2006) or from partial melting of the arc crust and assimilation of crustal material as also observed along mid-ocean ridges (Shukuno et al., 2006; Tamura and Tatsumi, 2002; Wanless et al., 2010). A third hypothesis is that they may also form by extensive fractional crystallisation of basaltic magmas (Arculus, 1994; Gill, 1981; Grove et al., 2005; Haase et al., 2006; Haase et al., 2011). Thus, silicic melts provide information on either the deeper subduction zone processes or, alternatively, on those that affect the ascending melts in the island arc at shallower crustal levels.

Silicic melts commonly erupt explosively which appears to be triggered by the injection of mafic melts into a shallow evolved magma chamber (Sparks et al., 1977; Woods and Cowan, 2009), but there is evidence that the injection of silicic melts can also trigger volcanic eruptions (de Silva et al., 2008). Silicic melts are also responsible for the formation of some of the largest volcanic calderas and frequent explosive eruptions observed in island arcs (Carey et al., 2018; Folch et al., 2001; Jellinek and DePaolo, 2003; Kawakami et al., 2007; Walker, 1984; Wright and Gamble, 1999). Thus, understanding the formation, evolution and ascent of melts from the mantle wedge through the island arc crust is important. The subsequent evolution and eruption from shallow magmatic systems (Kennedy et al., 2018; Self, 2006; Self and Blake, 2008), which may also consist of a complex systems of dykes and sills (c.f. Reid, 2014), is essential for the interpretation of silicic melt compositions and their eruptions. More recently, detailed investigations have questioned the simplicity of

the formation of island arc lavas resulting in explosive, evolved, volatile-rich eruptions. Kemner et al. (2015) showed that the submarine Monowai caldera volcano in the Tonga-Kermadec arc also contain relatively dry, tholeiitic melts that may have formed from mixing melts originating from both adiabatic decompression and fluid-fluxed melting. Hence, melts erupted in island arc calderas may contain crucial information on melt formation and ascent and may be better preserved in systems hosted in relatively thin island arc crust than in the thicker and more complex continental margin arcs (Ruprecht and Bachmann, 2010; Ruprecht and Plank, 2013).

The New Hebrides (Vanuatu) island arc consists of numerous volcanoes that frequently form islands situated in a tectonically complex arc-backarc system (Calmant, 2003; Meffre and Crawford, 2001; Mitchell and Warden, 1971; Ravenne et al., 1977; Taylor et al., 1995; Warden, 1967). Little is known about the composition and evolution of the submarine volcanoes and the impact of the local tectonic stress regime on magma geochemistry (Anderson et al., 2016). Submarine igneous samples from the arc and backarc volcanoes in the New Hebrides are rare (Crawford et al., 1988; Exon and Cronan, 1983; Greene and Exon, 1988; Lima et al., 2017; McConachy et al., 2005; Monjaret et al., 1991). The submarine Epi volcano consists of what has previously been interpreted to be a large submarine caldera supposedly hosting several post-caldera cones. In addition, Epi is situated in the transition zone between a compressional regime in the central New Hebrides arc (Calmant, 2003; Meffre and Crawford, 2001; Taylor et al., 1995) and an extensional regime in the south and thus provides the unique opportunity to investigate the processes and ascent of melts and their interaction with the local tectonic stress field.

Here, we use new major and trace element, and Sr-Nd-Pb isotope data of whole rocks and glasses from five submarine cones east of the island of Epi along with mineral major element chemistry. We show that the addition of sediment-derived fluids/melts released from the subducting slab along with fluids from the igneous slab have a significant impact on the

trace element compositions as expected in an island arc setting. We find no evidence for long-term petrologic disequilibria associated with magma mixing or assimilation within the lithosphere. The melts ascend through the crust in narrow pathways in a spatially limited area in which the impact from the surrounding host rocks and magmatic systems are small. The isolated ascent of the melts through the crust implies that the tectonic regime at Epi may prohibit establishment of a long-lived shallow magma chamber system. Instead the rising melts fractionate along a systems of dykes and sills continuously ascending and fractionating with little to no crustal assimilation.

2. GEOLOGICAL SETTING

The Vanuatu islands are part of the New Hebrides island arc system in the southwestern Pacific Ocean and started forming between the Eocene (Meffre and Crawford, 2001) and Middle Miocene due to the subduction of the Pacific Plate underneath the Australian Plate along the Vitiaz Trench (Schellart et al., 2006; Fig. 1). Collision of the Melanesian Border Plateau with the New Hebrides Ridge in the Middle Miocene caused a NE directed subduction of the South Fiji-North Loyalty Basin. Westward rollback of the subducting slab then led to a clockwise rotation of the New Hebrides arc and backarc extension associated with seafloor spreading in the North Fiji Basin from about 12 Ma (e.g., Schellart et al., 2006). The New Hebrides island arc is divided into three, independently moving blocks where the northern and southern segments are rotating counter-clockwise and clockwise, respectively, whereas the central block is moving eastward (Bergeot et al., 2009; Taylor et al., 1995; Vergniolle and Métrich, 2016). At present, the total rate of westward arc rollback of the southern Vanuatu arc increases from north to south (Schellart et al., 2006; Wallace et al., 2005). The presently active part of the island arc is the consequence of the subduction of the Australian Plate beneath the North Fiji Basin. Between 14°S and 17°S the Vanuatu Trench is unusually shallow due to the subduction of the D'Entrecasteaux Ridges and the West Torres

Massif (Fig. 1a) that also substantially affect the crustal structure of the central New Hebrides arc block (e.g., Bergeot et al., 2009; Meffre and Crawford, 2001). North and south of this central block, the arc started rifting about ~6 and ~3 Ma ago, respectively, opening the Jean Charcot Troughs in the north (Monjaret et al., 1991) and the Coriolis Troughs in the south (Fig. 1a; e.g., Dubois et al. (1977)) and forming the New Hebrides Ridge, a remnant section of the arc. The central block is undergoing compression as a result of collision with the D'Entrecasteaux Ridges and the West Torres Massif and most of the total plate convergence is accommodated by backarc thrusting (Fig. 1a; e.g., Taylor et al. (1995)). From north to south the recently active central New Hebrides island arc consists of the islands from Vanua Lava in the north to Anatom in the south (Monzier et al., 1997; Fig. 1a). All islands consist of several volcanic centres with the youngest ages typically at <1 Ma (Barsdell and Berry, 1990; Gorton, 1977).

The volcanic island of Epi is situated about 260 km south of the present intersection of the D'Entrecasteaux Ridge with the New Hebrides arc at the southern margin of the central block (Bergeot et al., 2009). However, 2-3 Ma ago, the D'Entrecasteaux Ridge may have entered the subduction zone at the recent latitude of Epi (Beaumais et al., 2013). Some 20 km northeast from Epi is the volcanically active island of Lopevi (Beaumais et al., 2013; Handley et al., 2008). The large Kuwae submarine caldera and Karua resurgent dome are situated towards the southeast of Epi and Tongoa (Fig. 1b). Tongoa was previously part of Epi island prior to a caldera-forming eruption at Kuwae in 1452 AD, which is assumed to have been one of the largest eruptions (Volcanic Eruption Index (VEI) 7) in historic times after the 1815 AD Tambora eruption (e.g., Goff and De Freitas, 2016; Monzier et al., 1994). Based on recent fieldwork, Németh et al. (2007) assigned the 1452 AD Kuwae eruption to be mainly submarine in origin and thus of much smaller (<VEI 6) magnitude of explosive eruptions. Today, Epi island hosts two structural provinces and numerous volcanic centres. The western part of Epi is formed by older raised marine and volcaniclastic strata and two Pliocene

volcanic structures (Barsdell and Berry, 1990; Quantin, 1972). The eastern part of Epi is formed almost exclusively from Quaternary volcanic rocks and has distinctive cliffs along its northeast shore, probably representing normal faults. The western wall has previously been interpreted to belong to a large submarine caldera system with a diameter of 9-15 km and water depths ranging from 400 to 500 m that was last active in 2004 (Garae et al., 2004). Our new bathymetric observations, however, question these observations and we will discuss the implication of these observations in more detail below. The area west of Epi island hosts at least seven smaller volcanic cones (each 1-2 km diameter) and three of these cones are aligned from west to east and have been named Epi A, B (recently being re-named Cioan volcano) and C (Greene and Exon, 1988), respectively (Fig. 1c). Historic volcanic activity at Epi has been described in 1920, 1953, 1960, 1984 and 2004 (Smithsonian Global Volcanism Project, (Greene and Exon, 1988). Four additional volcanic cones, named D to G are situated south of Epi B (Fig. 1c). Video imagery during the recent cruise reveals that all cones are covered by volcaniclastic material in various alteration stages, but only Cioan is covered by extremely fresh pumice and lava bombs (Haase et al., 2013). All cones exhibit evidence for previous hydrothermal activity (e.g., bacterial mats and Fe-Mn hydroxide staining) and during the recent cruise we found evidence for diffuse hydrothermal venting at the eastern flank of Cioan.

3. SAMPLING AND METHODS

The submarine Epi volcano was sampled during research cruise *SO-229 Coriolis Troughs* with the German RV Sonne in July 2013 (Table 1; Fig. 1). We sampled the Epi submarine cones during three dives (006-ROV, 013-ROV and 019-ROV) with the Remotely Operated Vehicle (ROV) Kiel 6000 from GEOMAR Helmholtz-Zentrum für Ozeanforschung Kiel. Dive 006-ROV approached the area between Cioan and Epi C from the south-east, dive 019-ROV targeted much of the area between the Cioan and Epi C edifices and dive 013-ROV was

performed from the area between Cioan and Epi C to the flank of Cioan and further south to Epi D. In addition, we performed eight successful TV-guided grabs (TVG) at Cioan and cones Epi C-G (008-TVG, 016-/017-TVG, 020-TVG, 023- to 026-TVG) from which igneous rock samples could be sampled. If fresh volcanic glass fragments (e.g., 006-ROV-11/-13) or matrix glasses (e.g., 006-ROV-01, 025-TVG-02) were available these were separated and analysed. For additional details of sample description see Haase et al. (2013)

For whole rock analyses, fresh cores were cut from the samples, coarsely crushed, washed thoroughly in deionised water to remove possible contamination from seawater, and then powdered in an agate mill at the GeoZentrum Nordbayern, Erlangen. The major element compositions of the matrix glasses and melt inclusions in clinopyroxene, orthopyroxene and plagioclase and the mineral compositions were analysed in thin sections using a JEOL JXA-8200 electron microprobe at the GeoZentrum Nordbayern, Erlangen. For glasses and melt inclusions the microprobe was operated with a 10 µm defocused beam, 15 nA beam current and a 15 kV acceleration voltage calibrated against natural standards (glass VG-A99 (NMNH 113498-1) for SiO_2, TiO_2, Al_2O_3, CaO, MgO, and FeO, glass VG-568 (NMNH 72854) for K_2O, scapolite (NMNH R6600-1) for Na_2O and Cl, chalcopyrite for S, rhodonite for MnO, apatite for P_2O_5). Precision and accuracy relative to A-99 were both better than 5 % (2σ) for all major elements (Beier et al., 2017; Brandl et al., 2012). The mineral analyses were performed using the same instrument operated at 15 nA, 15 kV with a fully focused beam (Freund et al., 2013). Calibration standards for mineral analyses were wollastonite (SiO_2, CaO), TiO_2, Al_2O_3, Fe_2O_3 (as FeO), rhodonite (MnO), MgO, albite (Na_2O), orthoclase (K_2O) and apatite (P_2O_5).

The whole rock sample powders are presented in supplemental Table 1 and their major element compositions were measured on fused glass beads on a Spectro XEPOS plus XRF spectrometer at the GeoZentrum Nordbayern, Erlangen (Freund et al., 2014). The major elements SiO_2, TiO_2, Al_2O_3, Fe_2O_3, MnO, MgO, Na_2O, K_2O, CaO, and P_2O_5 along with a

subset of trace elements (V, Cr, Co, Ni, Cu, Zn, Rb, Sr, Y, Zr, Nb, Ba) were analysed. Loss on ignition (LOI) was determined by weighing 1g of sample before and after heating the samples for 12 hours at 1300°C. Precision and accuracy of the major elements were generally better than 0.8% and 1% (2σ) for most elements and <0.5% for SiO_2.

The whole rock trace and glass trace elements were analysed by solution ICP-MS on a Thermo Scientific XSeries 2 quadrupole ICP-MS at the GeoZentrum Nordbayern, Erlangen. Sample powders and standards (BHVO-2, BCR-1) were dissolved following standard techniques using nitric and hydrofluoric acid as reactants (Freund et al., 2013; Lima et al., 2017). The samples were analysed at the same time than those presented in Lima et al. (2017) and standard values also apply to this dataset. Standards for major and trace element analyses are available in supplemental Table 2.

Radiogenic Sr and Nd isotopes were analysed at the GeoZentrum Nordbayern, Erlangen, following techniques described in Haase et al. (2017). Strontium and Nd isotope analyses were performed in static mode using a Thermo Fisher TRITON mass spectrometer with mass fractionation correction factors for $^{86}Sr/^{88}Sr = 0.1194$ and $^{146}Nd/^{144}Nd = 0.7219$. Repeated NBS SRM-987 standard measurements yielded $^{87}Sr/^{86}Sr$ of 0.710266 (2σ = 0.000024, n = 3). The reproducibility of the Erlangen Nd isotope standard gave an average of 0.511536 (2σ = 0.0000085, n = 2). The Erlangen Nd isotope standard has a $^{143}Nd/^{144}Nd$ = 0.511541 relative to the accepted value of 0.511850 for the LaJolla standard. The samples were normalised relative to the Erlangen Nd isotope standard.

Samples for Pb isotope analyses were dissolved using a HF-HNO_3 technique. Nitric and HCl acids were double distilled in order to minimise Pb blanks. Analyses were carried out using a ^{204}Pb-^{207}Pb double spike at the GeoZentrum Nordbayern using a Thermo Neptune Plus MC-ICP-MS. Spiked and unspiked aliquots were measured in static multi-collection mode. Standard runs of the NBS-981 standard (n = 14) gave average values of 16.9422 ±11, 15.4997 ±10, and 36.7239 ±25 for $^{206}Pb/^{204}Pb$, $^{207}Pb/^{204}Pb$ and $^{208}Pb/^{204}Pb$, respectively and

analyses of USGS BCR-2 standard yield 18.8139±7, 15.6334±6 and 38.7206±10 for $^{206}Pb/^{204}Pb$, $^{207}Pb/^{204}Pb$ and $^{208}Pb/^{204}Pb$, respectively. The major element, trace element, and Sr-Nd-Pb isotope data are presented in Table 1, all additional data are presented in supplemental Table 1.

4. PETROGRAPHY AND GEOCHEMISTRY

The Epi caldera samples range from pumiceous aphanitic samples with a glassy, cryptocrystalline vesicular groundmass (e.g., 017-TVG, 024-TVG-01) to relatively phyric, hypocrystalline textures (e.g., 026-TVG) to almost entirely phyric samples (e.g., 017-TVG-02) with varying amounts of a fine-grained to glassy groundmass (Fig. 2; (Haase et al., 2013)). All samples display evidence for extensive degassing, i.e. vesicularity may reach up to 30 vol.% with the vesicles often stretched implying flow textures. The prevailing mineral assemblage in all samples is plagioclase (up to 70 vol.%), olivine (~10 vol.%), clinopyroxene (~10 vol.%), and minor orthopyroxene, apatite and Fe-Ti-oxides (<10 vol.%). Several samples (e.g., 017-TVG-02) contain aggregates of olivine, clinopyroxene and orthopyroxene — the same mineral assemblage as in the groundmass (Fig. 2). Matrix glasses, glass embayments and glass inclusions occur frequently in the samples. Olivines from eight samples from Cioan, Epi G and Epi C (n=68) display almost constant forsterite (Fo = $100*Mg/(Mg+Fe^{2+})$) contents between cores and rims with a very subtle normal zoning and range from Fo 72 to 83 (average 79±2; Fig. 3). There is no systematic difference between olivine inclusions in plagioclase, matrix olivine, and olivine pheno- and antecrysts. Orthopyroxenes analysed in four samples from between cones Cioan and Epi C, at Epi D, and Epi G (n=38) displays almost no compositional zoning and have enstatite (En) contents from 55 to 64 (average 60±2) and ferrosilite (Fs) contents from 33 to 41 (average 36±2) and an average Mg# ($Mg\# = 100*Mg/(Mg+Fe^{T})$) of 63±2 (Fig. 3). Clinopyroxene phenocrysts in 9 samples from Epi C, Epi G, and Epi D (n= 168) range in wollastonite contents from 30 to 52

(average 42±3), enstatite ranges from 32 to 47 (average 42±2) and ferrosilite contents from 9 to 26 (average 16±4). They have an average Mg# of 72±6. Clinopyroxene crystals are normally zoned with slightly decreasing Mg# and enstatite contents from core to rim. A few crystals display minute changes (enstatite contents change by 2-3) between cores and rims that could be interpreted as inverse zonings. Since these changes are small we consider the overall compositions to be constant or normally zoned from cores to rims. Generally, olivine, orthopyroxene and clinopyroxene occurs in the more primitive lavas (i.e., those with whole rock SiO_2 contents <50 wt.%). However, the overall compositional range of the crystals in the mafic and silicic lavas is comparable (Fig. 3a). Plagioclase crystals from 9 samples from Cioan, Epi C, Epi G, and between Cioan and Epi C, (n= 199) display a much larger range in their compositions ranging in anorthite content (An = 100*(Ca/(Ca+Na+K))) between 31-96 (average 68±21), albite contents of 4-63 (average 31±19) and orthoclase contents up to 6 (average 2±1; Fig. 3). Plagioclase crystals with elevated An contents of >90 occur frequently (n= 50) either as large phenocrysts (>600 µm) or as inclusions (<20 µm) in clinopyroxene and as small crystals in the groundmass. Plagioclase crystals with An >52 frequently occur in lavas with <50 wt.% SiO_2 whereas lavas with SiO_2 >55 wt.% almost exclusively contain plagioclase crystals with An contents <50 (Fig. 3b).

The whole rock samples display a bimodal distribution with the majority of the samples at SiO_2 <50.3 wt.% and MgO contents of >5.9 wt.%; two more evolved whole rock lavas have ~62 wt.% SiO_2 and ~2 wt.% MgO (Fig. 4). The overall range of the whole rock major elements at Epi are similar to slightly larger than those at Lopevi (Beaumais et al., 2013), Ambrym (Handley et al., 2008; Sheehan and Barclay, 2016) or Efate (Raos and Crawford, 2004) at similar to slightly lower K_2O contents. Matrix glasses and glass inclusions have SiO_2 contents of >58.0 wt.% and MgO of <2.7 wt.% (Fig. 4). There is no clear systematic compositional difference between matrix glasses and glass inclusions analysed in clinopyroxene and plagioclase crystals. Hence, we suggest that post-entrapment crystallisation

and re-equilibration did not significantly alter the major element compositions of the glass inclusion for the purpose of this work. Generally, glass and whole rock compositions follow linear trends in most major elements, with the majority of the whole rocks at lower SiO_2, Na_2O and K_2O and higher MgO, FeO and CaO than the glasses.

Sulphur concentrations are generally below 350 ppm for all glasses but cover a large range and Cl/K ratios are generally below 0.1 (Fig. 5) with two samples extending towards 0.18 and Cl/Nb ratios are <700 (not shown, Table 1). Glasses and whole rock samples are enriched in incompatible Large Ion Lithophile Elements (LILE) and Light Rare Earth Elements (LREE) and depleted in Nb and Ta, respectively (Fig. 6 and 7). Europium anomalies expressed as Eu/Eu* (Eu/Eu* = $Eu_N/(Sm_N+Gd_N)$) are prominent in the more evolved lavas (Eu/Eu* <0.70) from the western cones (Fig. 7b). Lavas erupted at Epi C and G are more mafic (SiO_2 ~49 wt.%) and display less pronounced Eu anomalies (Eu/Eu* = 0.92-1.03). Fluid mobile elements (e.g., Ba, Rb, Pb) are enriched relative to the fluid immobile elements (e.g., Nb, Ta, Hf; Fig. 6). Generally, ratios of Ba/Nb, Th/Nb, and Zr/Nb do not correlate with fractionation indices (e.g., SiO_2 and MgO), and published subaerial data from eastern and western Epi cover a similar range but extend to more elevated Ba/Nb ratios (Fig. 7d-f). The Eu/Eu* and Tb/Yb ratios are correlated with SiO_2 (Fig. 7a-c). Despite comparable major elements, the Th/Nb ratios of Ambrym and Lopevi are lower than those from Epi, whereas Zr/Nb ratios are comparable to those from Lopevi but higher than those from Epi island and Ambrym (Fig. 7e). Ratios of Nb/Ta range from 14.7-20.7 for the new data from Epi caldera and are within the range of the literature data from Epi island (not shown).

The Sr-Nd-Pb isotope ratios of the Epi lavas display a bimodal distribution with two mafic lavas at slightly lower $^{206}Pb/^{204}Pb$ (026-TVG-01 and 026-TVG-05) and all other lavas at $^{206}Pb/^{204}Pb$ of ~18.49±0.02 (Fig. 8). Sample 026-TVG-01 also has lower $^{207}Pb/^{204}Pb$, $^{208}Pb/^{204}Pb$ (Fig. 8), and Ce/Pb but $^{87}Sr/^{86}Sr$ of 0.70422, whereas 026-TVG-05 only tends towards lower $^{208}Pb/^{204}Pb$ at lower $^{206}Pb/^{204}Pb$. $^{87}Sr/^{86}Sr$ isotope ratios range from 0.704197 to

0.704232 and the $^{143}Nd/^{144}Nd$ ratios range from 0.512938 to 0.512954. The trace element and radiogenic isotope ratios at Epi are not correlated, implying a decoupling of the isotope and trace element ratios during the evolution of the lavas.

4.1 THERMOBAROMETRIC CALCULATIONS

We performed a total of 122 thermobarometric calculations using clinopyroxenes, 40 of which were in equilibrium with the co-existing melt (supplemental Table 4 for details), the remaining analyses are clinopyroxene-only calculations. Additionally, 98 plagioclase crystals were used to calculate temperatures and pressures. Calculations were performed using equations 23 (Standard Error of Estimate (SEE) = ±43°C), 25a (SEE = ±0.38 GPa), 31 (SEE = ±0.29 GPa), 32a-32d (SEE = ±0.31 GPa, SEE = ±58°C), and 33 (SEE of calibration data = ±0.16 GPa) from Putirka (2008). We have used the pressures determined from the clinopyroxene barometers as input for the plagioclase calculations of the respective samples, however, it has to be noted that the pressure estimates from plagioclase equilibria have to be treated with caution (Putirka, 2008). In addition, we have calculated H_2O contents as estimated from plagioclase equilibria (Putirka, 2008) and compare these with plagioclase hygrometer results using minimum and maximum An contents available for the samples (Lange et al., 2009).

Pressures and temperatures for all Epi lavas straddle ~0.2 to ~0.7 GPa at temperatures ranging from 1,050°C to 1,250 °C (Fig. 9). We do not find evidence for specific depth levels of stagnation in the Epi lavas. Plagioclase barometric estimates display slightly higher pressures than calculated from clinopyroxene equilibria, however, this may be the result of a greater uncertainty of the plagioclase barometric estimates (Putirka, 2008). We note however, that the pressures calculated from clinopyroxene-glass equilibria, clinopyroxene and plagioclase crystals overlap within their intra-sample variability and uncertainty (Putirka, 2008) and range between 8-30 km depth, well within the estimated range of crustal thickness

for the region around Epi (Monzier et al., 1997). The calculated H_2O contents, using plagioclase-liquid equilibria (Putirka, 2008) in lavas with <50.3 wt.% SiO_2, range from 2-4 wt.% (Fig. 9c). The more evolved lavas display a bimodal distribution with a group of samples at H_2O contents <2 wt.% and one sample deviating to contents of 4-5 wt.%.

5. DISCUSSION

5.1 PRIMITIVE MELTS AND SOURCE COMPOSITIONS AT EPI

The formation and modification of melts in subduction zones has been subject of numerous studies (Arculus, 1994; Gill, 1981; Pearce et al., 1995; Pearce and Parkinson, 1993; Pearce and Peate, 1995; Plank and Langmuir, 1993; Porter and White, 2009; Regelous et al., 1997; Tatsumi and Eggins, 1995; Tatsumi and Kogiso, 2003; Todd et al., 2012) and the general geochemical characteristics of the Epi lavas are similar to those of other subduction zone lavas (c.f. Pearce and Peate, 1995). An enrichment in fluid-mobile elements (e.g., Ba, Rb, Pb) is combined with subtly low immobile High Field Strength Element (HFSE) concentrations and ratios (e.g., Nb/Ta = 14.7-20.7, Nb/Zr = 0.020-0.025; MORB: 16.8±1.2 and 0.062±0.058, respectively (Jenner and O'Neill, 2012); Fig. 6). The HFSE contents of the Epi lavas resemble the lowest concentrations observed in Pacific MORB (Fig. 6) and imply that the mantle underneath the islands has experienced previous melt depletion and that Lopevi and Epi lavas originate from a mantle source in which much of the trace element variability can best be explained by addition of a subducting sedimentary component (Fig. 7; Peate et al., 1997). We note however, that these differences are subtle and may reflect minor heterogeneities of the mantle wedge. The depleted mantle wedge has subsequently been re-enriched by a water-rich component derived from the subducting slab. Slightly elevated water contents are also consistent with the plagioclase-liquid estimates (Fig. 9). We note however, that radiogenic isotopes are not correlated with either fluid- or depletion-sensitive trace element ratios in the Epi lavas, implying that depletion must have been relatively recently (Pearce and Peate, 1995;

Peate et al., 1997) and that a long-term compositional heterogeneity of the mantle wedge may not affect the lava trace element compositions. Instead wedge depletion and addition of fluids is likely to result from the recent subduction process (Fig. 6). The exact origin of chemical depletion of the central New Hebrides island arc mantle wedge remains unclear in the absence of a nearby backarc (Pearce and Peate, 1995; Peate et al., 1997). The elevated Th/Nb ratios in the submarine Epi lavas compared to the subaerial Epi as well as Lopevi and Ambrym lavas indicate that fluids underneath Epi not only originate from the igneous portion of the slab, but may also inherit a trace element signature from the subducting sediments (Pearce and Peate, 1995; Plank, 2005). The fractionation of Ba/Nb and Th/Nb of Lopevi could also be explained by fluid addition from altered oceanic crust (Fig. 7), but Lopevi, Ambrym and Epi lavas display elevated $^{87}Sr/^{86}Sr$, $^{207}Pb/^{204}Pb$ and $^{208}Pb/^{204}Pb$ similar to those observed in the subducting sediments (Peate et al., 1997; Plank and Langmuir, 1993). Despite the uncertainty in sedimentary compositions entering the New Hebrides island arc the elevated Ba/Nb, Th/Nb, Nb/La and, to a lesser extent, Zr/Nb ratios may best be explained by mobilisation from the subducting sedimentary portion of the slab. The contribution from the sedimentary subduction component is volumetrically small (5-10%, see modelling in Fig. 7), but significantly impacts on the depleted mantle wedge composition as a result of the higher elemental concentrations. The fractionation of Ba and Nb can be explained using a volcaniclastic sedimentary composition (Peate et al., 1997; Plank and Langmuir, 1993) along with partition coefficients at 800°C and 1000°C (Fig. 7; Kessel et al., 2005). The relatively high temperatures imply that the sedimentary component may be added as a melt rather than a fluid.

Slab depths at Epi caldera are on the order of 200 km, similar to those proposed for Ambrym and Lopevi but range from 140 to 160 km underneath Epi island (Fig. 1b; Hayes et al., 2012). At these depths the slab surface temperatures are on the order of 800-900°C (Syracuse et al., 2010), high enough to result in partial melting of sediments (Hermann and

Rubatto, 2009; Hermann and Spandler, 2008; Spandler and Pirard, 2013) in agreement with our best model fit. The occurrence of stronger sedimentary signatures at Epi compared to Ambrym and Lopevi (Fig. 7) may reflect shallower levels of dehydration and partial melting of the subducting sedimentary components at Epi compared to the neighbouring volcanoes (Beaumais et al., 2013; Pearce et al., 2007). The majority of the trace element ratios (e.g., Eu/Eu*, Ce/Yb, Tb/Yb; Fig. 7) are correlated with SiO_2 contents, thus suggesting that shallow level crustal processes may have significantly affected the compositions of the melt products erupted at Epi the significance of which we will discuss in detail below.

5.2 MELT EVOLUTION AT CRUSTAL LEVELS

Previous works have stressed the importance of crustal assimilation and fractional crystallisation in the New Hebrides arc lavas (Beaumais et al., 2013; Handley et al., 2008). The Epi glasses and whole rocks cover a wide range in SiO_2 and MgO (Fig. 4) and contain numerous normally zoned clinopyroxene and plagioclase crystals (Fig. 3), suggesting that the melts were modified by fractional crystallisation. The fact that the lavas follow linear trends for incompatible elements like K and Zr with increasing SiO_2, as well as the constant compositions of Sr isotopes across the entire range of SiO_2, suggests that the Epi samples lie on one single liquid line of descent (Fig. 4 and Fig. 7). The difference between the whole rock and glass compositions and the presence of mafic xenocrysts is indicative that much of the major element variability may best be explained by xeno- and antecryst accumulation, and crystal aggregation in the lavas. Even the most primitive glass of the Epi lavas at 58 wt.% SiO_2 and 3.4 wt.% MgO (sample 006-ROV-13) has experienced extensive fractionation processes relative to a primitive, mantle-derived melt.

Decreasing Eu/Eu*, and increasing Nb/Yb and $(Ce/Yb)_N$ with increasing SiO_2 show that some incompatible element ratios have been significantly affected by fractional

crystallisation (Fig. 7) or, in the case of the whole rock samples by addition of xeno- and antecrysts (see also Monzier et al., 1997). Olivines lack a zoning pattern and have relatively low Fo contents (Fo 72-83 in equilibrium with mantle melts that have Mg# 44-60 (Roeder and Emslie, 1970)) and therefore, they are not in equilibrium with mantle melts or residual mantle (Green et al., 2001; Herzberg and Asimow, 2008; Niu and O'Hara, 2007)(Fig. 3b). Instead, these must have fractionated from a more mafic, parental melt (Mg# of ~72 if in equilibrium with the mantle) that is not directly sampled by one of the Epi submarine cones (Mg# of erupted magmas: 18-40). Similarly, the clinopyroxenes have relatively evolved compositions not in equilibrium with clinopyroxene from the mantle (Mg# ~91; (Putirka, 2008))**.** It has to be noted that the number of clinopyroxenes with relatively high Mg# decreases towards the more evolved rocks (Fig. 3a) indicative for a continuous crystal fractionation.

The frequent occurrence of plagioclase with An >90 could be related to elevated H_2O contents in the magma (Sisson and Grove, 1993). Plagioclase xenocrysts with An contents >70 have Ca/Na ratios ranging from 4-35 and both glasses and melt inclusions ranging from 58.1 to 70 wt.% SiO_2 display Ca/Na ratios of 0.5-2.5. These elevated Ca/Na ratios could be indicative of total H_2O contents of >2 wt.% in the Epi melts (Sisson and Grove, 1993) and our plagioclase hygrometer results could imply similarly elevated H_2O contents (Fig. 9). However, Danyushevsky et al. (1997) showed that high-An plagioclase can also crystallise from dacitic melts saturated in H_2O at shallow pressures and does not necessarily require a primary melt with elevated H_2O content. We can show that our high An-contents almost exclusively occur in the mafic lavas (Fig. 3) making crystallisation from a silicic melt unlikely. We also note that the majority of high-An plagioclase crystals are normally zoned with significantly lower An contents at their rims (e.g., in sample 026-TVG-07) consistent with an origin from fractional crystallisation. Based on the major element sums of >98 wt.%, high vesicularity of lavas, and our H_2O estimations on the most primitive sample using the plagioclase hygrometer (Fig. 9c), we suggest that the melts have minimum H_2O contents of 2-

2.5 wt.%. Such H_2O contents are lower than typical mafic arc magmas (cf. Plank et al., 2013) consistent with our observation that the Ba/Nb and Ba/Yb are elevated when being compared to MORB, but are relatively low compared to other island arc volcanoes. Instead the ratios at Epi are more comparable to those commonly found in backarc lavas (Pearce and Stern, 2006).

The general lack of sieve textures, resorption or re-crystallisation rims and the prevalent occurrence of normally zoned clinopyroxene and plagioclase implies that mixing between evolved and basaltic magmas did not influence the melts significantly during their ascent. We observe that sample 024-TVG-01, situated in the hydrothermal area between Cioan and Epi C (Fig. 1c), has two distinct glass compositions that range in SiO_2 between ~60 to ~70 wt.% which implies that the melts did not homogenise. Nevertheless, we do not observe systematic differences between each of the cones sampled. Sulphur concentrations range up to 350 ppm S and overlap with concentrations found in other subduction zone settings (Haase et al., 2006). The values suggest that the melts have experienced significant amounts of degassing (Brounce et al., 2014). The relatively low Cl/K ratios of the glasses provide evidence that little interaction with the surrounding seawater occurred. Combined with our petrographic observations we suggest that the lavas have experienced relatively little crustal assimilation or melt mixing modifications during ascent and eruption but have been subject to significant fractional crystallisation and degassing from a parental mafic magma. These observations, combined with the sparse occurrence of complex disequilibrium textures (e.g., absence of sieve textures, oscillating mineral zonings and recrystallized rims) and our thermobarometric estimates (Fig. 9), suggest that melts have not stagnated in the crust at any specific level and/or for any long period of time.

The trace elements (e.g., low Eu/Eu*, Nb/Yb, high $(Ce/Yb)_N$) and heavy REE (e.g., Dy/Yb_N) at Epi could reflect amphibole differentiation (supplemental Figs. S1 and S2; Davidson et al., 2007; Davidson et al., 2012). Marcelot et al. (1983) found a few amphiboles in andesitic lavas from Futuna and Sorbadere et al. (2011) conclude that lavas from Aoba may

contain a component derived from amphibole-bearing clinopyroxenite sources. Amphibole-bearing cumulates are possibly stored at lower crustal levels (>800 MPa) similar to those observed at Merapi (Peters et al., 2017). The potential deep crystallization and storage of amphibole in subduction magmas (Davidson et al., 2007) poses the question as to why lavas from Epi do not contain any evidence for amphibole or biotite in their crystallising assemblage, neither in the mafic or evolved lavas and mafic mineral agglomerates. The thermobarometry at Epi suggests that the Epi lavas crystallise over a relatively large range of pressures, from ~0.7 GPa to ~0.2 GPa (Fig. 9). Our rhyolite-MELTS modelling suggests that the large range in SiO_2 contents (46.1-70.2 wt.%) at Epi can be best explained by shallow level crystallisation at relatively high temperatures, likely in excess of 1000°C (Fig. 4 and 9). Crystallisation temperatures are thus too high to facilitate crystallisation of amphibole (Ridolfi et al., 2010). Furthermore, H_2O contents as calculated from plagioclase-liquid equilibria suggest that H_2O contents are too low to result in the fractionation of amphibole (e.g., Krawczynski et al., 2012). Instead, the observed trace element pattern can be explained by differentiation of significant amounts of clinopyroxene, which is in agreement with our petrographic observations, $(Ce/Yb)_N$, $(Dy/Yb)_N$ and Dy/Dy* ratios (Figs. S1 and S2) and systematically decreasing CaO/Al_2O_3 ratios with increasing SiO_2 (Fig. S2). In conclusion, the predominant crystallisation of clinopyroxene as opposed to amphibole suggest that crystallization dominantly occurs at shallow levels (<1 GPa; Ridolfi and Renzulli, 2012) and at high temperatures (Ridolfi et al., 2010), where amphibole stability is significantly reduced as the melts approach the surface (Rutherford and Hill, 1993). Thus, the Epi fractionation assemblage consists of olivine, clinopyroxene, orthopyroxene, plagioclase and Fe-Ti oxides with no chemical or petrographical evidence for amphibole or biotite.

5.3 Tectonic and Magmatic Implications: Evidence for a Submarine Caldera?

The original interpretation that the submarine eastern Epi volcano is a caldera system was based on a geophysical survey in 1984. Greene and Exon (1988) and Crawford et al. (1988) suggested that the three large submarine cones Epi A-C are aligned on the northern rim of a submerged caldera (Fig. 10a). According to their interpretation of seismic profiles, the submarine ridge extending northwards from southeastern Epi island represents the eastern caldera wall. One observation is that the submarine Epi volcanic cones form a stack of edifices of varying age. However, in 2004, the French Institut de Recherche pour le Développement (IRD) undertook a high resolution bathymetric survey of the area and Pelletier et al. (2004) concluded that the Epi A-C cones are not located on the margin of a caldera. Their new bathymetric data along with data collected during cruise SO-229 indicate that the submarine ridge previously interpreted to be the caldera wall may be in fact a fault structure that strikes roughly N-S (Fig. 1c) and has a normal or slight right-lateral trans-tensional shear sense. This structure may represent a major lineament that extends southwards from the rear-arc thrust further north (Fig. 10a). A large submarine canyon breaches this fault-bounded ridge and is the locus of extensive mass transport from around the Epi submarine cones onto the eastern slopes of the island arc. The seismic profile (cf. Fig. 6 of Crawford et al., 1988) previously interpreted as caldera wall and floor could thus also be interpreted as a fault-bounded ridge and accumulation of layered volcaniclastic sediments upslope of the narrow gorge cross-cutting the ridge. On land, we used the publicly available SRTM (Shuttle Radar Topographic Mission) 1 arc-second data to identify possible fault trends. The main trend of fault scarps on the western part of the island of Epi is roughly 150-160°, whereas on the eastern part, fault scarps rotate towards more easterly directions (~100-110°; Fig. 10). From the fault scarps observed on land, there is no evidence for a subaerial continuation of the

submerged caldera structure as previously suggested (Fig. 10). Thus, at present, there is no compelling seismic, structural or bathymetric evidence for the existence of a submerged caldera at Epi. However, a complete bathymetric survey, especially north of Epi will be required to unravel the morphological and structural relationships of the submarine and subaerial Epi volcanic and tectonic structures.

Our new thermobarometric calculations for the submarine Epi lavas preclude the presence of a stable shallow magma reservoir, in which magmas stagnate for prolonged periods of time (Bachmann and Bergantz, 2008; Bachmann and Huber, 2016) emphasizing the possible lack of a crustal magma chamber system underlying a hypothesized Epi caldera. Instead, the polybaric crystallization indicated in lavas from all cones of Epi encompasses almost the entire crustal thickness underneath Epi (Monzier et al., 1997). This suggests that the melts ascend through a complex system of sills and dikes (c.f. Annen et al., 2015; Reid, 2014) in which melts continuously rise from Moho depths (~30 km) to shallower levels of ~8 km or less. Comparable observations were made in the Taupo volcanic zone by Gamble et al. (1999) and in the southern Cascades by Brophy and Dreher (2000). Thus, our petrological evidence for the lack of pro-longed melt stagnation at a given pressure interval (i.e., a stable magma reservoir) is another argument to question the existence of a caldera system at Epi (c.f. Kennedy et al., 2018) as opposed to the neighbouring Kuwae caldera.

5.4 Links between regional Tectonics and Volcanism

Regional tectonics may control melt ascent paths and storage in volcanic arcs (Chaussard and Amelung, 2014; Hughes and Mahood, 2008) and we consider the New Hebrides island arc to be no exception. The New Hebrides island arc is subdivided into three major segments displaying differences in total convergence and relative motion rate (Taylor et al., 1995). The central segment is moving east relative to the northern and southern segments due to the collision of the D'Entrecasteaux Ridges and the West Torres Massif that is also

responsible for rear-arc thrusting along the central arc segment (Fig. 1). The relative motion between the central and the neighbouring northern and southern arc segments, respectively, is accommodated by strike-slip zones and especially the motion of the southern segment is well constrained by GPS motion vectors and earthquake focal mechanisms (Pelletier et al., 1998; Taylor et al., 1995). This dextral strike-slip zone is of great importance for the volcanic systems of Ambrym, Lopevi, Epi and Kuwae/Karua, that form the volcanically most active part of the arc (Picard et al., 1994). Ambrym, with its 12 km wide caldera and the resurgent domes of Marum and Benbow is located exactly at the transition from regional subsidence in the South Aoba Basin (collapse of the central arc due to collisional uplift in the forearc and thrusting in the rear-arc; (Meffre and Crawford, 2001)) to strike-slip faulting (Picard et al., 1994). Lopevi, Epi and Kuwae/Karua are all located within the strike-slip zone as proposed by Taylor et al. (1995).

The formation of the Epi lavas by continuous fractional crystallisation contrasts with observations from nearby Lopevi volcano (Beaumais et al., 2013; Handley et al., 2008). These differences may provide additional constraints on Epi's specific tectonic setting. In contrast to the roughly E-W trending strike-slip zone of Taylor et al. (1995), Meffre and Crawford (2001) proposed two distinct strike-slip faults oriented ~45° and cross-cutting the arc. These extend from the trench to Ambrym and Epi, respectively cf. Fig. 12 of Meffre and Crawford (2001)). Here, we suggest that at Ambrym the orientation of the strike-slip zone is roughly E-W in accordance with the major rift intersecting the whole island and the seismic zone south of Ambrym (Fig. 10b). At Epi and on the seafloor SW of Epi, a series of lineaments have been mapped displaying two major strike orientations at ~70° and ~45° (Fig. 10b). This, in combination with the two roughly N-S trending major lineaments (Fig. 10a), may result in a highly fractured and permeable crust. Additionally, Epi is situated not only at the tip point of reversal in lateral but also of vertical crustal motions. According to Meffre and Crawford (2001), the whole area between Ambrym and Efate is affected by uplift, whereas the backarc

(rifting/spreading) and forearc (gravitational collapse following northward migration of collision with the D'Entrecasteaux Ridges) are subsiding south of Epi. North of Ambrym the central section of the arc system (North and South Aoba Basins) is subsiding whereas the fore- and rear-arc crust is being uplifted.

The structural regime of the New Hebrides island arc between Ambrym and the Vate Trough can be interpreted as a dextral strike-slip zone with a complex subset of Riedel shears (Fig. 11a). Changes in stress field from compression to extension (plus rotation) result in a variety of active shear systems (Fig. 11a) with different orientations. In Fig. 11b, we applied this model to the natural system with the result of a consistent structural interpretation of the morphological, seismic and volcanic lineaments mapped at Epi (Fig. 10b).

Even though Epi is located on relatively thick (~30 km) arc crust, the lithosphere is likely to be intensely weakened and fractured and may thus suppress the formation of a shallow, stable magma reservoir. Instead, the system of normal and strike-slip faults and shears supports the formation of dykes and sills (Reid, 2014). The ascent of magmas through a complex system of dykes and sills results in only limited mixing between individual melt batches (Fig. 11c). The small scale major element variability in individual volcanic edifices but similar trace element compositions between different cones may be indicative of a common magma reservoir with melts being extracted at different times. This also explains the alignment of the Epi cones and most other volcanic lineaments between Ambrym and the Vate Trough along synthetic shear bands (Fig. 11b) and stresses the importance of tectonic structures on the melting regime and melt ascent in island arc systems (Anderson et al., 2016; Lima et al., 2017). Interestingly, comparable observations of a tectonic influence in the production and ascent of magma "packages" were recently made at Ruapehu Volcano in the Taupo volcanic zone, New Zealand (Conway et al., 2018).

CONCLUSIONS

Lavas erupted at Epi volcano in the New Hebrides arc display a wide range from mafic whole rock compositions to evolved groundmass glass and glass inclusions. The lavas rise through thick island arc crust but have experienced little interaction with the neighbouring magmatic systems, which have experienced substantial assimilation of crustal material. This could be due to the fact that the wall rocks to these dyke and sill-like conduits may be "armoured" by crystallization from the magma. We conclude that much of the overall petrological character of the Epi lavas is the result of the specific tectonic setting of Epi, situated between two distinct structural domains. The compressional regime in the north and the extensional regime in the south may result in a highly fractured and thus permeable lithosphere that allows the ascent of isolated, distinctive melt batches through a complex system of dykes and sills. These isolated ascent pathways are situated in a broad strike-slip zone that originates from the regional scale tectonic evolution of the New Hebrides arc. The geochemical signatures indicate that the initial mafic melts formed from a slightly depleted mantle wedge by addition of fluids and melts from igneous and sedimentary portions of the slab, respectively. A lack of amphibole and biotite in the mineral assemblage of Epi suggests that crystals formed from a melt not sufficiently saturated in H_2O and/or at temperatures above amphibole stability. Thus, the petrology and geochemistry of silicic, relatively volatile-poor melts in island arcs may be substantially influenced by shallow, crustal processes rather than deep mantle signatures. The continuous range in pressures observed at Epi is inconsistent with a significant and stable magma stagnation in crustal reservoirs but rather indicates a polybaric magmatic system consisting of dykes and sills which also explains the lack of evidence for mixing and assimilation as would be the case in a large, crustal magma chamber. Our observations may also be applicable to other oceanic arcs, especially those that are situated in a complex tectonic regime. Our work stresses the importance of interdisciplinary studies able to connect geological and structural observations with geochemistry.

ACKNOWLEDGMENTS

We acknowledge captain D. Korte and his crew of R/V Sonne and the ROV Kiel 6000 crew for their invaluable help and remarkable efforts during SO-229 and thank the entire scientific party for their immense efforts. PAB thanks N. Augustin and M. Le Saout for their valuable help during multibeam processing and GIS data compilation, we thank S. Meffre for his helpful suggestions and IFREMER for providing additional bathymetric data. We kindly thank M. Regelous and B. Storch for their help in the Erlangen isotope laboratories. We acknowledge support by the Smithsonian Institution in providing calibration and measurement standards for the microprobe analyses. We thank T. Rooney in the Tokyo Haneda ANA Lounge, and J. Gamble for their constructive and helpful reviews that have improved the manuscript considerably and acknowledge constructive comments and editorial handling by A. Kerr. We acknowledge funding of the Bundesministerium für Bildung und Forschung (BMBF) for funding the cruise through project 03G0229A and thank T. Tevi, H. Cook and T. McConachy for their invaluable logistic help from the Australian to the Vanuatu shores and Coriolis Troughs. ChB acknowledges inspirational support from the peaty south coast of Islay. We dedicate this manuscript to Jon Davidson an inspiring, friendly and humorous scientist and colleague.

REFERENCES

Adam, J., Rushmer, T., O'Neil, J., Francis, D., 2012. Hadean greenstones from the Nuvvuagittuq fold belt and the origin of the Earth's early continental crust. Geology 40, 363-366, doi:10.1130/G32623.1

Anderson, M.O., Hannington, M.D., Haase, K., Schwarz-Schampera, U., Augustin, N., McConachy, T.F., Allen, K., 2016. Tectonic focusing of voluminous basaltic eruptions in magma-deficient backarc rifts. Earth and Planetary Science Letters 440, 43-55, doi:10.1016/j.epsl.2016.02.002

Annen, C., Blundy, J.D., Leuthold, J., Sparks, R.S.J., 2015. Construction and evolution of igneous bodies: Towards an integrated perspective of crustal magmatism. Lithos 230, 206-221, doi:10.1016/j.lithos.2015.05.008

Arculus, R., 1999. Origins of the continental crust. Journal and Proceedings - Royal Society of New South Wales 132, 83-110

Arculus, R.J., 1994. Aspects of magma genesis in arcs. Lithos 33, 189-208, doi:10.1016/0024-4937(94)90060-4

Bachmann, O., Bergantz, G.W., 2008. Rhyolites and their Source Mushes across Tectonic Settings. Journal of Petrology 49, 2277-2285, doi:10.1093/petrology/egn068

Bachmann, O., Huber, C., 2016. Silicic magma reservoirs in the Earth's crust. American Mineralogist 101, 2377-2404

Baillard, C., Crawford, W.C., Ballu, V., Regnier, M., Pelletier, B., Garaebiti, E., 2015. Seismicity and shallow slab geometry in the central Vanuatu subduction zone. Journal of Geophysical Research-Solid Earth 120, 5606-5623, doi:10.1002/2014jb011853

Ballu, V., Calmant, S., 2004. Campagne VATATERM du N.O. Alis au Vanuatu.

Barsdell, M., Berry, R.F., 1990. Origin and Evolution of Primitive Island-Arc Ankaramites from Western Epi, Vanuatu. Journal of Petrology 31, 747-777

Beaumais, A., Chazot, G., Dosso, L., Bertrand, H., 2013. Temporal source evolution and crustal contamination at Lopevi Volcano, Vanuatu Island Arc. Journal of Volcanology and Geothermal Research 264, 72-84, doi:10.1016/j.jvolgeores.2013.07.005

Beier, C., Haase, K.M., Brandl, P.A., Krumm, S.H., 2017. Primitive andesites from the Taupo Volcanic Zone formed by magma mixing. Contributions to Mineralogy and Petrology 172, 33, doi:10.1007/s00410-017-1354-0

Bergeot, N., Bouin, M.N., Diament, M., Pelletier, B., Régnier, M., Calmant, S., Ballu, V., 2009. Horizontal and vertical interseismic velocity fields in the Vanuatu subduction zone from GPS measurements: Evidence for a central Vanuatu locked zone. Journal of Geophysical Research: Solid Earth 114, doi:10.1029/2007JB005249

Brandl, P.A., Beier, C., Regelous, M., Abouchami, W., Haase, K.M., Garbe-Schönberg, D., Galer, S.J.G., 2012. Volcanism on the flanks of the East Pacific Rise: Quantitative constraints on mantle heterogeneity and melting processes. Chemical Geology 289-299, 41-56, doi:10.1016/j.chemgeo.2011.12.015

Brophy, J.G., Dreher, S.T., 2000. The origin of composition gaps at South Sister volcano, central Oregon: implications for fractional crystallization processes beneath active calc-alkaline volcanoes. Journal of Volcanology and Geothermal Research 102, 287-307, doi:10.1016/S0377-0273(00)00192-X

Brounce, M.N., Kelley, K.A., Cottrell, E., 2014. Variations in Fe3+/∑Fe of Mariana Arc Basalts and Mantle Wedge fO2. Journal of Petrology 55, 2513-2536, doi:10.1093/petrology/egu065

Calmant, S., 2003. New insights on the tectonics along the New Hebrides subduction zone based on GPS results. Journal of Geophysical Research 108, 22

Carey, R., Soule, S.A., Manga, M., White, J.D.L., McPhie, J., Wysoczanski, R., Jutzeler, M., Tani, K., Yoerger, D., Fornari, D., Caratori-Tontini, F., Houghton, B., Mitchell, S., Ikegami, F., Conway, C., Murch, A., Fauria, K., Jones, M., Cahalan, R., McKenzie, W., 2018. The largest deep-ocean silicic volcanic eruption of the past century. Science Advances 4

Castillo, P.R., Lonsdale, P.F., Moran, C.L., Hawkins, J.W., 2009. Geochemistry of mid-Cretaceous Pacific crust being subducted along the Tonga-Kermadec Trench: Implications for the generation of arc lavas. Lithos 112, 87-102, doi:10.1016/j.lithos.2009.03.041

Chaussard, E., Amelung, F., 2014. Regional controls on magma ascent and storage in volcanic arcs. Geochemistry, Geophysics, Geosystems 15, doi:10.1002//2013GC005216

Conway, C., Gamble, J.A., Wilson, C.J.N., Leonard, G.S., Townsend, B., Calvert, A.T., 2018. New petrological, geochemical and geochronological perspectives on andesite-dacite magma gensis at Ruapehu volcano, New Zealand. American Mineralogist 103, doi:10.2138/am-2018-6199

Crawford, A.J., Greene, H.G., Exon, N.F., 1988. Geology, petrology and geochemistry of submarine volcanoes around Epi island, New Hebrides island arc, in: Greene, H.G., Wong,

F.L. (Eds.), Geology and offshore resources of Pacific Island Arcs-Vanuatu region. Cirum-Pacific Council for Energy and Mineral Resources, pp. 301-327.

Danyushevsky, L.V., Carroll, M.R., Falloon, T.J., 1997. Origin of High-An Plagioclase in Tongan High-Ca boninites: implications for plagicolase-melt equilibria at low P(H_2O). The Canadian Mineralogist 35, 313-326

Davidson, J., Turner, S., Handley, H., Macpherson, C., Dosseto, A., 2007. Amphibole "sponge" in arc crust? Geology 35, 787-790

Davidson, J., Turner, S., Plank, T., 2012. Dy/Dy*: Variations Arising from Mantle Sources and Petrogenetic Processes. 525-537, doi:10.1093/petrology/egs076

de Silva, S., Salas, G., Schubring, S., 2008. Triggering explosive eruptions - The case for silicic magma recharge at Huaynaputina, southern Peru. Geology 36, 387-390

Dubois, J., Lille, R., Montadert, L., 1977. Geodynamics in the southwest Pacific. Eos, Transactions American Geophysical Union 58, 1109-1109, doi:10.1029/EO058i012p01109

Dupuy, C., Dostal, J., Marcelot, G., Bougault, H., Joron, J.L., Treuil, M., 1982. Geochemistry of Basalts from Central and Southern New Hebrides Arc - Implication for Their Source Rock Composition. Earth and Planetary Science Letters 60, 207-225, doi:10.1016/0012-821x(82)90004-8

Eissen, J.-P., 1996. CALVA cruise. RV L'Atalante, doi:10.17600/96010050

Exon, N.F., Cronan, D.S., 1983. Hydrothermal iron deposits and associated sediments from submarine volcanoes off Vanuatu, southwest Pacific. Marine Geology 52, M43-M52, doi:10.1016/0025-3227(83)90052-X

Folch, A., Codina, R., Marti, J., 2001. Numerical modeling of magma withdrawal during explosive caldera-forming eruptions. Journal of Geophysical Research 106, 16163-16175

Freund, S., Beier, C., Krumm, S., Haase, K.M., 2013. Oxygen isotope evidence for the formation of andesitic–dacitic magmas from the fast-spreading Pacific–Antarctic Rise by assimilation–fractional crystallisation. Chemical Geology 347, 271-283, doi:10.1016/j.chemgeo.2013.04.013

Freund, S., Haase, K., Keith, M., Beier, C., Garbe-Schönberg, D., 2014. Constraints on the formation of geochemically variable plagiogranite intrusions in the Troodos Ophiolite, Cyprus. Contributions to Mineralogy and Petrology 167, 1-22, doi:10.1007/s00410-014-0978-6

Gamble, J.A., Wood, C.P., Price, R.C., Smith, I.E.M., Stewart, R.B., Waight, T., 1999. A fifty year perspective of magmatic evolution on Ruapehu Volcano, New Zealand: verification of open system behaviour in an arc volcano. Earth and Planetary Science Letters 170, 301-314

Garae, E., Todman, S., Charley, D., 2004. Rapport de l'éruption du 16-24 février 2004 du volcan sous marin "East Epi". Department of Geology, Mines and Water Resources, Section of Volcanology and Geo-Hazards Management, p. 14.

Ghiorso, M.S., Gualda, G.A.R., 2015. An H2O–CO2 mixed fluid saturation model compatible with rhyolite-MELTS. Contributions to Mineralogy and Petrology 169, 53, doi:10.1007/s00410-015-1141-8

Gill, J.B., 1981. Orogenic Andesites and Plate Tectonics. Springer, Berlin

Goff, J.R., De Freitas, C.R., 2016. Natural hazards in Australasia. Cambridge University Press

Gorton, M.P., 1977. The geochemistry and origin of quaternary volcanism in the New Hebrides. Geochimica et Cosmochimica Acta 41, 1257-1270, doi:10.1016/0016-7037(77)90071-0

Green, D., Falloon, T., Eggins, S., Yaxley, G., 2001. Primary magmas and mantle temperatures. European Journal of Mineralogy 13, 437-451

Greene, H.G., Exon, N.F., 1988. Acoustic stratigraphy and hydrothermal activity within Epi Submarine Caldera, Vanuatu, New Hebrides Arc. Geo-Marine Letters 8, 121-129, doi:10.1007/BF02326088

Grove, T.L., Baker, M.B., Price, R.C., Parman, S.W., Elkins-Tanton, L.T., Chatterjee, N., Muntener, O., 2005. Magnesian andesite and dacite lavas from Mt. Shasta, northern California: products of fractional crystallization of H2O-rich mantle melts. Contributions to Mineralogy and Petrology 148, 542-565, doi:10.1007/s00410-004-0619-6

Gualda, G.A.R., Ghiorso, M.S., Lemons, R.V., Carley, T.L., 2012. Rhyolite-MELTS: a Modified Calibration of MELTS Optimized for Silica-rich, Fluid-bearing Magmatic Systems. Journal of Petrology 53, 875-890, doi:10.1093/Petrology/Egr080

Haase, K.A., Stroncik, N., Garbe-Schönberg, D., Stoffers, P., 2006. Formation of island are dacite magmas by extreme crystal fractionation: An example from Brothers Seamount, Kermadec island arc (SW Pacific). Journal of Volcanology and Geothermal Research 152, 316-330, doi:10.1016/j.jvolgeores.2005.10.010

Haase, K.M., Beier, C., Regelous, M., Rapprich, V., Renno, A., 2017. Spatial variability of source composition and petrogenesis in rift and rift flank alkaline lavas from the Eger Rift, Central Europe. Chemical Geology, doi:10.1016/j.chemgeo.2016.11.003

Haase, K.M., Koschinsky, A., Schwarz-Schampera, U., Abegg, F., Abegg, J., Allen, K., Anderson, M.O., Beier, C., Bodendorfer, M., Bühring, B., Brandl, P.A., Cuno, P., Franke, H., Garbe-Schönberg, D., Greß, M., Hannington, M.D., Haruel, C., Hennke, J., Huusmann, H., Kemner, F., Kleint, C., Kuckuck, J., Nasemann, P., Pieper, M., Rose, J., Suck, I., 2013. Volcanism, hydrothermal activity and vent biology in the Coriolis Troughs, New Hebrides Island Arc; RV Sonne cruise SO-229, Cruise report / Fahrtbericht, 01.07.2013, Townsville (Australia) to 26.07.2013, Nouméa (New Caledonia). GeoZentrum Nordbayern, Universität Erlangen-Nürnberg, 1-86, doi:10.2312/cr_so229

Haase, K.M., Krumm, S., Regelous, M., Joachimski, M., 2011. Oxygen isotope evidence for the formation of silicic Kermadec island arc and Havre-Lau backarc magmas by fractional crystallization rather than crustal re-melting Earth and Planetary Science Letters 309, 348-355, doi:10.1016/j.epsl.2011.07.014

Hall, R., Spakman, W., 2002. Subducted slabs beneath the eastern Indonesia-Tonga region: insights from tomography. Earth and Planetary Science Letters 201, 321-336

Handley, H.K., Turner, S.P., Smith, I.E.M., Stewart, R.B., Cronin, S.J., 2008. Rapid timescales of differentiation and evidence for crustal contamination at intra-oceanic arcs: Geochemical and U-Th-Ra-Sr-Nd isotopic constraints from Lopevi Volcano, Vanuatu, SW Pacific. Earth and Planetary Science Letters 273, 184-194

Hayes, G.P., Wald, D.J., Johnson, R.L., 2012. Slab1. 0: A three-dimensional model of global subduction zone geometries. Journal of Geophysical Research 117, B01302, doi:10.1029/2011JB008524, 2012

Hermann, J., Rubatto, D., 2009. Accessory phase control on the trace element signature of sediment melts in subduction zones. Chemical Geology 265, 512-526, doi:10.1016/j.chemgeo.2009.05.018

Hermann, J., Spandler, C.J., 2008. Sediment Melts at Sub-arc Depths: an Experimental Study. Journal of Petrology 49, 717-740

Herzberg, C., Asimow, P.D., 2008. Petrology of some oceanic island basalts: PRIMELT2.XLS software for primary magma calculation. Geochemistry, Geophysics, Geosystems 9, doi:10.1029/2008GC002057

Hughes, G.R., Mahood, G.A., 2008. Tectonic controls on the nature of large silicic calderas in volcanic arcs. Geology 36, 627-630

Jellinek, A.M., DePaolo, D.J., 2003. A model for the origin of large silicic magma chambers: precursors of caldera-forming eruptions. Bulletin of Volcanology 65, 363-381, doi:10.1007/s00445-003-0277-y

Jenner, F., O'Neill, H., 2012. Analysis of 60 elements in 616 ocean floor basaltic glasses. Geochemistry Geophysics Geosystems 13, Q02005, doi:10.1029/2011GC004009

Kawakami, Y., Hoshi, H., Yamaguchi, Y., 2007. Mechanism of caldera collapse and resurgence: Observations from the northern part of the Kumano Acidic Rocks, Kii peninsula, southwest Japan. Journal of Volcanology and Geothermal Research 167, 263-281

Kemner, F., Haase, K.M., Beier, C., Krumm, S., Brandl, P.A., 2015. Formation of andesite melts and Ca-rich plagioclase in the submarine Monowai volcanic system, Kermadec arc. Geochemistry, Geophysics, Geosystems 16, 4130-4152, doi:10.1002/2015GC005884

Kennedy, B.M., Holohan, E.P., Stix, J., Gravley, D.M., Davidson, J., Cole, J.W., 2018. Magma plumbing beneath collapse caldera volcanic systems. Earth-Science Reviews, doi:10.1016/j.earscirev.2017.12.002

Kessel, R., Schmidt, M.W., Ulmer, P., Pettke, T., 2005. Trace element signature of subduction-zone fluids, melts and supercritical liquids at 120-180 km depth. Nature 437, 724-727, doi:10.1038/nature03971

Krawczynski, M.J., Grove, T.L., Behrens, H., 2012. Amphibole stability in primitive arc magmas: effects of temperature, H2O content, and oxygen fugacity. Contributions to Mineralogy and Petrology 164, 317-339, doi:10.1007/s00410-012-0740-x

Lallemand, S., Heuret, A., Boutelier, D., 2005. On the relationships between slab dip, back-arc stress, upper plate absolute motion, and crustal nature in subduction zones. Geochemistry Geophysics Geosystems 6, Q09006, doi:10.1029/2005gc000917

Lange, R.A., Frey, H.M., Hector, J., 2009. A thermodynamic model for the plagioclase-liquid hygrometer/thermometer. American Mineralogist 94, 494-506, doi:10.2138/am.2009.3011

Laporte, C., Briqueu, L., Cluzel, D., Eissen, J.P., 1998. Isotopic gradient along the New Hebrides arc (Vanuatu, SW Pacific). Collision of the d'Entrecasteaux Zone and heterogeneity of mantle sources. Comptes Rendus De L Academie Des Sciences Serie Ii Fascicule a-Sciences De La Terre Et Des Planetes 326, 101-106, doi:10.1016/S1251-8050(97)87453-8

Lima, S.M., Haase, K.M., Beier, C., Regelous, M., Brandl, P.A., Hauff, F., Krumm, S., 2017. Magmatic Evolution and Source Variations at the Nifonea Ridge (New Hebrides Island Arc). Journal of Petrology 58, 473-494, doi:10.1093/petrology/egx023

Lyubetskaya, T., Korenaga, J., 2007. Chemical composition of Earth's primitive mantle and its variance: 1. Method and results. Journal of Geophysical Research 112, B03211, doi:10.1029/2005JB004223

Marcelot, G., Dupuy, C., Girod, M., Maury, R.C., 1983. Petrology of Futuna Island Lavas (New Hebrides) - an Example of Calc-Alkaline Magmatism Associated with the Initial-Stages of Back-Arc Spreading. Chemical Geology 38, 23-37, doi:10.1016/0009-2541(83)90043-8

McConachy, T.F., Arculus, R.J., Yeats, C.J., Binns, R.A., Barriga, F.J.A.S., McInnes, B.I.A., Sestak, S., Sharpe, R., Rakau, B., Tevi, T., 2005. New hydrothermal activity and alkalic volcanism in the backarc Coriolis Troughs, Vanuatu. Geology 33, 61-64

McDonough, W.F., Sun, S.-S., 1995. The composition of the Earth. Chemical Geology 120, 223-253

Meffre, S., Crawford, A.J., 2001. Collision tectonics in the New Hebrides arc (Vanuatu). Island Arc 10, 33-50, doi:10.1046/j.1440-1738.2001.00292.x

Mitchell, A.H.G., Warden, A.J., 1971. Geological evolution of the New Hebrides island arc. Journal of the Geological Society 127, 501-529

Monjaret, M.C., Bellon, H., Maillet, P., 1991. Magmatism of the troughs behind the New Hebrides island arc (RV Jean Charcot SEAPSO 2 cruise): K-Ar geochronology and petrology. Journal of Volcanology and Geothermal Research 46, 265-280, doi:10.1016/0377-0273(91)90088-H

Monzier, M., Robin, C., Eissen, J.-P., Cotten, J., 1997. Geochemistry vs. seismo-tectonics along the volcanic New Hebrides Central Chain (Southwest Pacific). Journal of Volcanology and Geothermal Research 78, 1-29, doi:10.1016/S0377-0273(97)00006-1

Monzier, M., Robin, C., Eissen, J.P., 1994. Kuwae (≈1425 Ad) - the Forgotten Caldera. Journal of Volcanology and Geothermal Research 59, 207-218, doi:10.1016/0377-0273(94)90091-4

Németh, K., Cronin, S.J., White, J.D.L., 2007. Kuwae Caldera and Climate Confusion. The Open Geology Journal 1, 7-11

Niu, Y., O'Hara, M.J., 2007. Global Correlations of Ocean Ridge Basalt Chemistry with Axial Depth: a New Perspective. Journal of Petrology 49, 633-644, doi:10.1093/petrology/egm051

Patriat, M., Collot, J., Danyushevsky, L., Fabre, M., Meffre, S., Falloon, T., Rouillard, P., Pelletier, B., Roach, M., Fournier, M., 2015. Propagation of back-arc extension into the arc

lithosphere in the southern New Hebrides volcanic arc. Geochemistry Geophysics Geosystems 16, 3142-3159, doi:10.1002/2015gc005717

Pearce, J.A., Baker, P.E., Harvey, P.K., Luff, I.W., 1995. Geochemical Evidence for Subduction Fluxes, Mantle Melting and Fractional Crystallization Beneath the South Sandwich Island Arc. Journal of Petrology 36, 1073-1109

Pearce, J.A., Kempton, P.D., Gill, J.B., 2007. Hf-Nd evidence for the origin and distribution of mantle domains in the SW Pacific. Earth and Planetary Science Letters 260, 98-114

Pearce, J.A., Parkinson, I.J., 1993. Trace element models for mantle melting: application to volcanic arc petrogenesis. Geological Society, London, Special Publications 76, 373-403, doi:10.1144/GSL.SP.1993.076.01.19

Pearce, J.A., Peate, D.W., 1995. Tectonic Implications of the Composition of Volcanic Arc Magmas. Annual Review of Earth and Planetary Sciences 23, 251-285, doi:10.1146/annurev.ea.23.050195.001343

Pearce, J.A., Stern, R.J., 2006. The origin of back-arc basin magmas: trace element and isotope perspectives., in: Christie, D.M. (Ed.), Back-Arc Spreading Systems: Geological, Biological, Chemical, and Physical Interactions, Washington D.C., pp. 63-86.

Peate, D.W., Pearce, J.A., Hawkesworth, C.J., Colley, H., Edwards, C.M.H., Hirose, K., 1997. Geochemical variations in Vanuatu arc lavas: the role of subducted material and a variable mantle wedge composition. Journal of Petrology 38, 1331-1358, doi:10.1093/petrology/38.10.1331

Pelletier, B., Bani, P., Calmant, S., Ballu, V., Garaebiti, E., Todman, S., Charley, D., McConachy, T.F., 2004. Epi (Vanuatu) - Seamount with repeated eruptions and uncertain history, but stable summit elevation. Bulletin of the Global Volcanism Network - Smithsonian National Museum of National History 29, 1-4

Pelletier, B., Calmant, S., Pillet, R., 1998. Current tectonics of the Tonga-New Hebrides region. Earth and Planetary Science Letters 164, 263-276

Pertermann, M., Hirschmann, M.M., 2003. Anhydrous Partial Melting Experiments on MORB-like Eclogite: Phase Relations, Phase Compositions and Mineral-Melt Partitioning of Major Elements at 2-3 GPa. Journal of Petrology 44, 2173-2201

Peters, S.T.M., Troll, V.R., Weis, F.A., Dallai, L., Chadwick, J.P., Schulz, B., 2017. Amphibole megacrysts as a probe into the deep plumbing system of Merapi volcano, Central Java, Indonesia. Contributions to Mineralogy and Petrology 172, 16, doi:10.1007/s00410-017-1338-0

Picard, C., Monzier, M., Eissen, J.P., Robin, C., 1994. Concomitant evolution of tectonic environment and magma geochemistry, Ambrym volcano (Vanuatu, New Hebrides arc). Geological Society, London, Special Publications 81, 135

Plank, T., 2005. Constraints from Thorium/Lanthanum on sediment recycling at subduction zones and the evolution of the continents. Journal of Petrology 46, 921-944

Plank, T., Kelley, K.A., Zimmer, M.M., Hauri, E.H., Wallace, P.J., 2013. Why do mafic arc magmas contain ~4wt% water on average? Earth and Planetary Science Letters 364, 168-179, doi:10.1016/j.epsl.2012.11.044

Plank, T., Langmuir, C.H., 1993. Tracing trace elements from sediment input to volcanic output at subduction zones. Nature 362, 739-743

Polat, A., 2012. Growth of Archean continental crust in oceanic island arcs. Geology 40, 383-384, doi:10.1130/focus042012.1

Porter, K.A., White, W.M., 2009. Deep mantle subduction flux. Geochem. Geophys. Geosyst. 10, Q12016, doi:10.1029/2009gc002656

Putirka, K.D., 2008. Thermometers and Barometers for Volcanic Systems. Minerals, Inclusions and Volcanic Processes 69, 61-120, doi:10.2138/rmg.2008.69.3

Quantin, P., 1972. Geological Map of Epi. Office de la recherche scientifique et technique outre-mer centre de Noumea, Noumea.

Raos, A.M., Crawford, A.J., 2004. Basalts from the Efate Island Group. central section of the Vanuatu arc, SW Pacific, geochemistry and petrogenesis. Journal of Volcanology and Geothermal Research 134, 35-56

Ravenne, C., Pascal, G., Dubois, J., Dugas, F., Montadert, L., 1977. Model of a young intra-oceanic arc: the new Hebrides island arc, International Symposium on geodynamics in south-west Pacific Noumea (New Caledonia). Editions Technip, Paris, Noumea, pp. 63-78.

Regelous, M., Collerson, K.D., Ewart, A., Wendt, J.I., 1997. Trace element transport rates in subduction zones; evidence from Th, Sr and Pb isotope data for Tonga-Kermadec Arc lavas. Earth and Planetary Science Letters 150, 291-302

Reid, M.R., 2014. Timescales of Magma Transfer and Storage in the Crust, in: Turekian, K.K. (Ed.), Treatise on Geochemistry (Second Edition). Elsevier, Oxford, pp. 181-201.

Ridolfi, F., Renzulli, A., 2012. Calcic amphiboles in calc-alkaline and alkaline magmas: thermobarometric and chemometric empirical equations valid up to 1,130°C and 2.2 GPa. Contributions to Mineralogy and Petrology 163, 877-895, doi:10.1007/s00410-011-0704-6

Ridolfi, F., Renzulli, A., Puerini, M., 2010. Stability and chemical equilibrium of amphibole in calc-alkaline magmas: an overview, new thermobarometric formulations and application to subduction-related volcanoes. Contributions to Mineralogy and Petrology 160, 45-66, doi:10.1007/s00410-009-0465-7

Roeder, P.L., Emslie, R.F., 1970. Olivine-liquid equilibrium. Contributions to Mineralogy and Petrology 29, 275-289

Ruprecht, P., Bachmann, O., 2010. Pre-eruptive reheating during magma mixing at Quizapu volcano and the implications for the explosiveness of silicic arc volcanoes. Geology 38, 919-922, doi:10.1130/G31110.1

Ruprecht, P., Plank, T., 2013. Feeding andesitic eruptions with a high-speed connection from the mantle. Nature 500, 68-72, doi:10.1038/nature12342

Rutherford, M.J., Hill, P.M., 1993. Magma ascent rates from amphibole breakdown; an experimental study applied to the 1980-1986 Mount St. Helens eruptions. Journal of Geophysical Research, B, Solid Earth and Planets 98, 19,667-619,685

Ryan, W.B.F., Carbotte, S.M., Coplan, J.O., O'Hara, S., Melkonian, A., Arko, R., Weissel, R.A., Ferrini, V., Goodwillie, A., Nitsche, F., Bonczkowski, J., Zemsky, R., 2009. Global Multi-Resolution Topography synthesis. Geochemistry, Geophysics, Geosystems 10, doi:10.1029/2008GC002332

Schellart, W.P., Lister, G.S., Toy, V.G., 2006. A Late Cretaceous and Cenozoic reconstruction of the Southwest Pacific region: Tectonics controlled by subduction and slab rollback processes. Earth-Science Reviews 76, 191-233, doi:10.1016/j.earscirev.2006.01.002

Self, S., 2006. The effects and consequences of very large explosive volcanic eruptions. Philosophical Transactions of the Royal Society A: Mathematical, Physical and Engineering Sciences 364, 2073

Self, S., Blake, S., 2008. Consequences of explosive supereruptions. Elements 4, 41-46, doi:10.2113/Gselements.4.1.41

Sheehan, F., Barclay, J., 2016. Staged storage and magma convection at Ambrym volcano, Vanuatu. Journal of Volcanology and Geothermal Research 322, 144-157, doi:10.1016/j.jvolgeores.2016.02.024

Shukuno, H., Tamura, Y., Tani, K., Chang, Q., Suzuki, T., Fiske, R.S., 2006. Origin of silicic magmas and the compositional gap at Sumisu submarine caldera, Izu–Bonin arc, Japan. Journal of Volcanology and Geothermal Research 156, 187-216, doi:10.1016/j.jvolgeores.2006.03.018

Sisson, T.W., Grove, T.L., 1993. Experimental investigations of the role of H_2O in calc-alkaline differentiation and subduction zone magmatism. Contributions to Mineralogy and Petrology 113, 143-166

Smith, I.E.M., Worthington, T.J., Price, R.C., Stewart, R.B., Maas, R., 2006. Petrogenesis of dacite in an oceanic subduction environment: Raoul Island, Kermadec arc. Journal of Volcanology and Geothermal Research 156, 252-265, doi:10.1016/j.jvolgeores.2006.03.003

Sorbadere, F., Schiano, P., Métrich, N., Garaebiti, E., 2011. Insights into the origin of primitive silica-undersaturated arc magmas of Aoba volcano (Vanuatu arc). Contributions to Mineralogy and Petrology 162, 995-1009, doi:10.1007/s00410-011-0636-1

Spandler, C., Pirard, C., 2013. Element recycling from subducting slabs to arc crust: A review. Lithos 170-171, 208-223, doi:10.1016/j.lithos.2013.02.016

Sparks, S.R.J., Sigurdsson, H., Wilson, L., 1977. Magma mixing: a mechanism for triggering acid explosive eruptions. Nature 267, 315-318

Stracke, A., Bizimis, M., Salters, V.J.M., 2003. Recycling oceanic crust: Quantitative constraints. Geochemistry, Geophysics, Geosystems 4, Q8003, doi:10.1029/2001GC000223

Syracuse, E.M., van Keken, P.E., Abers, G.A., 2010. The global range of subduction zone thermal models. Physics of the Earth and Planetary Interiors 183, 73-90, doi:10.1016/j.pepi.2010.02.004

Tamura, Y., Tatsumi, Y., 2002. Remelting of an andesitic crust as a possible origin for rhyolitic magma in oceanic arcs: an example from the Izu-Bonin arc. Journal of Petrology 43, 1029-1047

Tatsumi, Y., Eggins, S.M., 1995. Subduction Zone Magmatism. Blackwell

Tatsumi, Y., Kogiso, T., 2003. The subduction factory: its role in the evolution of the Earth's crust and mantle. Geological Society, London, Special Publications 219, 55-80, doi:10.1144/gsl.sp.2003.219.01.03

Taylor, F.W., Bevis, M.G., Schutz, B.E., Kuang, D., Recy, J., Calmant, S., Charley, D., Regnier, M., Perin, B., Jackson, M., Reichenfeld, C., 1995. Geodetic measurements of convergence at the New Hebrides island arc indicate arc fragmentation caused by an impinging aseismic ridge. Geology 23, 1011-1014, doi:10.1130/0091-7613(1995)023<1011:GMOCAT>2.3.CO;2

Taylor, S.R., Capp, A.C., Graham, A.L., Blake, D.H., 1969. Trace element abundances in andesites. Contributions to Mineralogy and Petrology 23, 1-26, doi:10.1007/BF00371329

Todd, E., Gill, J.B., Pearce, J.A., 2012. A variably enriched mantle wedge and contrasting melt types during arc stages following subduction initiation in Fiji and Tonga, southwest Pacific. Earth and Planetary Science Letters, 180-194

Vergniolle, S., Métrich, N., 2016. A bird's eye view of "Understanding volcanoes in the Vanuatu arc". Journal of Volcanology and Geothermal Research 322, 1-5, doi:10.1016/j.jvolgeores.2016.08.012

Walker, G.P.L., 1984. Downsag calderas, ring faults, caldera sizes, and incremental caldera growth. Journal of Geophysical Research. 89, 8407-8416

Wallace, L.M., McCaffrey, R., Beavan, J., Ellis, S., 2005. Rapid microplate rotations and backarc rifting at the transition between collision and subduction. Geology 33, 857-860

Wanless, V.D., Perfit, M.R., Ridley, W.I., Klein, E., 2010. Dacite Petrogenesis on Mid-Ocean Ridges: Evidence for Oceanic Crustal Melting and Assimilation. Journal of Petrology 51, 2377-2410

Warden, A.J., 1967. The geology of the Central Island: New Hebrides. Geological Survey Report 5

Woods, A.W., Cowan, A., 2009. Magma mixing triggered during volcanic eruptions. Earth and Planetary Science Letters 288, 132-137

Workman, R.K., Hart, S.R., 2005. Major and trace element composition of the depleted MORB mantle (DMM). Earth and Planetary Science Letters 231, 53-72, doi:10.1016/j.epsl.2004.12.005

Wright, I.C., Gamble, J.A., 1999. Southern Kermadec submarine caldera arc volcanoes (SW Pacific): caldera formation by effusive and pyroclastic eruption. Marine Geology 161, 207-227

FIGURE CAPTIONS

Fig. 1. a) Overview Map of the New Hebrides (Vanuatu) island arc. Tectonic structures in a) are from (Meffre and Crawford, 2001) and Patriat et al. (2015). Convergence rates are in cm/year from Calmant (2003). Grid in a) is from GEBCO (IHO-IOC GEBCO Gazetteer of Undersea Feature Names, www.gebco.net). Note that overall slap dip in the New Hebrides (Vanuatu) island arc may be amongst the steepest observed (~70°; (Lallemand et al., 2005) (Hall and Spakman, 2002)) but is varying from <15° over the first 20-40 km to 40° at 40 km depth (Baillard et al., 2015). b) bathymetry of the Epi, Ambrym and Lopevi region using a GMRT grid (Ryan et al., 2009) as background, and high-resolution ship based data from expeditions SO229 (Haase et al., 2013), CALVA (Eissen, 1996) and digitised grids from VATATERM (Ballu and Calmant, 2004). Subaerial elevation model compiled from ASTER Global Digital Elevation Model (GDEM) v2 data. ASTER GDEM is a product of NASA and METI. Depth of the Vanuatu Slab (Hayes et al., 2012) is shown by the coloured contour lines. Other symbols as in a). c) submarine cones east of Epi. Bathymetric grid compiled from GEBCO, high-resolution ship based data from expedition SO229 (Haase et al., 2013), and digitised grids from VATATERM (Ballu and Calmant, 2004). Note that sampling area in c) is on the same length scale than that of Ruapehu volcano in the Taupo volcanic zone discussed in Conway et al. (2018).

Fig. 2. Representative thin section images from submarine Epi caldera samples. a) sample 008-TVG-01g in plane polarised light with large clinopyroxene crystal and groundmass consisting mainly of Fe-Ti oxides, b) sample 017-TVG-01 in plane polarised light, with large clinopyroxene and plagioclase aggregate. Groundmass consists of glass and Fe-Ti oxides. Few small anhedral olivine crystals are also observed in the matrix. c) 017-TVG-02 in crossed polarised light showing phyric sample consisting of large clinopyroxene, plagioclase and olivine crystals, d) sample 017-TVG-07 in plane polarised light showing large aggregate of clinopyroxene and plagioclase in a glassy groundmass, e) vesicular sample 024-TVG-01 in

plane polarised light with large plagioclase crystal in glassy groundmass, and d) sample 026-TVG-01 under crossed polarised light with large clinopyroxene and plagioclase aggregate in fine grained matrix of clinopyroxene, olivine and plagioclase.

Fig. 3. a) Mg# numbers of clinopyroxene, orthopyroxene and olivine crystals. b) Anorthite (An) contents of plagioclase crystals versus SiO_2 contents of whole rock samples. Note the occurrence of a limited amount of high An and high Mg# crystals in the silicic lavas providing evidence for the occurrence of mafic xenocrysts in the more evolved lavas.

Fig. 4. Major element variation diagrams of whole rocks, matrix glasses and glass inclusions of the submarine Epi caldera. Panels a-f include non-normalised mineral analyses, panels g-l contain rhyolite-MELTS models (Ghiorso and Gualda, 2015; Gualda et al., 2012) calculated using sample 026-TVG-05 as starting composition. We use sample 026-TVG-05 as the most primitive sample that may best represent a liquid equivalent. This particular sample is sparsely phyric, hypocrystalline with ~10% plagioclase phenocrysts and 1-2% sub-rounded to subangular olivines in a fine-grained matrix (Haase et al., 2013).

Curves shown were calculated with fractionate solids flag using varying water contents and QFM buffer settings (Model A: 0.25 wt.% H_2O, 70 MPa, QFM; Model B: 0.25 wt.% H_2O, 70 MPa, QFM+1; Model C: 1.5 wt.% H_2O, 70 MPa, QFM; Model D: 1.5 wt.% H_2O, 70 MPa, QFM+1). A model calculated at 800 MPa fails to reproduce compositions at >55 wt.% SiO_2 (not shown). Tick marks in models in panels g-l are rhyolite-MELTS temperature steps of 25°C. Literature data for eastern and central Epi are from Dupuy et al. (1982) and data for western Epi are from Gorton (1977), Dupuy et al. (1982), Barsdell and Berry (1990) and Pearce et al. (2007) for a single sample. For analytical methods see main text.

Fig. 5. Cl/K ratios and S concentrations of the Epi matrix glass and glass inclusions and embayments. Note that two samples extent towards Cl/K ratios of 0.18 (at ~100 ppm S) not show in this figure. Arrows mark potential impact from assimilation of crustal material (increasing Cl/K) and degassing (lowering S), respectively. Limit of detection (l.o.d.) of S inferred from mineral calibration standard (see main text).

Fig. 6. a) Primitive mantle (PRIMA) normalized trace element abundance pattern and b) normal mid-ocean ridge basalt (N-MORB) normalized Rare Earth Element pattern of Epi whole rocks and glasses. PRIMA from Lyubetskaya and Korenaga (2007), N-MORB from McDonough and Sun (1995). Literature data from Gorton (1977), Barsdell and Berry (1990) and Pearce et al. (2007). Note the distinct depletions in immobile source sensitive elements (e.g., Nb, Ta) and enrichments in fluid mobile elements (e.g., Ba, Rb, Pb). Pacific MORB data compiled from Jenner and O'Neill (2012).

Fig. 7. a) Nb/Yb, b) Eu/Eu* and c) $(Ce/Yb)_N$ ratios versus SiO_2 contents; d) Th/Nb, e) Zr/Nb and f) Nb/La versus Ba/Nb ratios of the Epi glasses and whole rock data. Epi literature data as in figure 3, Ambrym data from Gorton (1977), Peate et al. (1997) and Pearce et al. (2007) Lopevi data from Beaumais et al. (2013) and Handley et al. (2008). Pacific MORB data compiled from Jenner and O'Neill (2012). Melt from depleted MORB mantle calculated using 10% fractional spinel peridotite melting of a depleted MORB mantle source provided by Workman and Hart (2005). Partition coefficients are those compiled and presented by Stracke et al. (2003). Subduction components (SC) sources calculated using partition coefficients by Kessel et al. (2005) for 1000°C (SC^1) and 800°C (SC^2). Altered oceanic crust from Castillo et al. (2009), fluid calculated at 700°C Kessel et al. (2005). Subducting, dehydrating and melting sediments are compiled in Plank and Langmuir (1993) from Peate et al. (1997). Tick marks are 0%, 5% followed by 10% intervals of adding a sediment fluid/melt to a DMM

composition. Note that the range in Nb/La ratios in Figure 7f is slightly influenced by fractional crystallisation (i.e. mafic whole rocks ranging from 0.15-0.2, more silicic glasses are at ~0.25).

Fig. 8. a) $^{87}Sr/^{86}Sr$, b) $^{207}Pb/^{204}Pb$ and c) $^{208}Pb/^{204}Pb$ versus $^{206}Pb/^{204}Pb$ ratios of the Epi glasses and whole rocks. Literature data as in Figure 3 and 6. Pacific MORB data are those compiled from Stracke et al. (2003). Epi literature data are from Laporte et al. (1998), Lopevi from Beaumais et al. (2013), Ambrym and sediment data from Peate et al. (1997). Note however, that as a result of scarcity of data the sediment composition may contain some uncertainty.

Fig. 9. a) Temperatures and pressures from clinopyroxene only and clinopyroxene-liquid equilibria and plagioclase-liquid thermobarometers summarised in Putirka (2008), b) temperatures versus whole rock SiO_2 contents and c) calculated H_2O contents based on plagioclase-liquid equilibria after Putirka (2008). Arrows in c) show degassing and fractional crystallisation trends respectively. Whole rock thermobarometric data are averages from mineral calculations. Note that uncertainties of the calculations are 0.26-0.31 GPa and 46°C for clinopyroxene-liquid and clinopyroxene calculations and ±0.38 GPa and ±43°C for plagioclase-liquid calculations (Putirka, 2008). Note that pressure estimates from plagioclase depend on input pressures previously determined by clinopyroxene barometry. Here, only those pressures are being used where a common agreement between clinopyroxene and plagioclase calculations exists. Note, however, that the pressure estimates from plagioclase-liquid equilibria have to be considered with caution.

Fig. 10. a) Tectonomagmatic map of the area around Epi. Volcanic edifices and fault have been mapped using bathymetric and topographic data also used in Fig. 1b) plus additional bathymetric data from RV Southern Surveyor cruise CoTroVe in 2004 (Arculus et al., 2004)

for the Vate Trough. The proposed outline of Epi caldera from Greene & Exon (1988) is shown by the dashed, dark red line. b) Structural map of the area between Ambrym and Efate. Earthquake data were downloaded from the USGS earthquake catalogue (http://earthquake.usgs.gov) for reviewed earthquakes (1960-2017) with magnitude >4.5 at depths of <30 km. Lineaments mapped based on seismicity are shown in white, those based on morphology in pink and those based on volcanism in yellow.

Fig. 11. a) Model of a dextral shear zone in a compressional and extensional setting. Riedel shears R (synthetic) and R' (antithetic), and the secondary synthetic P shears. b) Application of the model in a) to the New Hebrides arc area between Ambrym and Efate. Note that the synthetic Riedel shears may be focusing volcanic activity (yellow dashed lines), the antithetic Riedel shears may be accommodating most of the extensional movement (normal faulting) and the secondary synthetic P shears may form a subset of major crustal lineaments visible in morphological changes (pink). c) Synthesis sketch of melting, melt ascent and tectonic focusing underneath Epi. Not to scale.

TABLE HEADINGS

Table 1. Representative whole rock and glass major element, trace element and Sr-Nd-Pb isotope data. Full dataset for glasses, glass inclusions and minerals available in supplemental Tables 1 and 3. Methods as described in the main text. Whole rock major element analyses performed by XRF, trace element analyses of glasses and whole rock samples by solution ICP-MS at the GeoZentrum Nordbayern, Friedrich-Alexander Universität Erlangen-Nürnberg following methods also described in Lima et al. (2017). Major elements of the glasses were determined using an electron microprobe. International Geo Sample Numbers (IGSN) registered at System for Earth Sample Registration (SESAR, http://geosamples.org). Errors

for spiked Pb analyses are generally ±0.002, ±0.0019 and ±0.0046 for $^{206}Pb/^{204}Pb$, $^{207}Pb/^{204}Pb$ and $^{20}8Pb/^{204}Pb$, respectively.

SUPPLEMENTAL MATERIAL

Supplemental Table 1. Whole rock, glass major element, trace element and Sr-Nd-Pb isotope dataset. International Geo Sample Numbers (IGSN) registered at System for Earth Sample Registration (SESAR, http://geosamples.org). Original, shipboard sampling labels refer to 'Station/Sampling locality (see Fig. 1) - Sampling Method (see main text) - Individual sample number', i.e. TVG samples were taken by TV grab, ROV samples were taken during dives with Remotely Operated Vehicle Kiel 6000. Whole rock major element analyses performed by XRF, trace element analyses of glasses and whole rock samples by solution ICP-MS at the GeoZentrum Nordbayern, Friedrich-Alexander Universität Erlangen-Nürnberg following methods also described in Lima et al. (2017). Major elements of the glasses were determined using an electron microprobe. Errors for spiked Pb analyses are generally ±0.002, ±0.0019 and ±0.0046 for $^{206}Pb/^{204}Pb$, $^{207}Pb/^{204}Pb$ and $^{208}Pb/^{204}Pb$, respectively.

Supplemental Table 2. Standard data for major and trace element analyses of whole rocks and glasses and electron microprobe standard for mineral analysis.

Supplemental Table 3. Mineral data of the Epi lavas. International Geo Sample Numbers (IGSN) registered at System for Earth Sample Registration (SESAR, http://geosamples.org). Parent IGSN refers to whole rock samples presented in Table 1 and supplemental Table 1.

Supplemental Table 4. Mineral data of the Epi lavas for those samples for which pressures and temperatures were calculated using Putirka (2008). International Geo Sample Numbers

(IGSN) registered at System for Earth Sample Registration (SESAR, http://geosamples.org). Parent IGSN refers to whole rock samples presented in Table 1 and supplemental Table 1.

Supplemental Fig. S1. Fractionation models of clinopyroxene and amphibole for chondrite normalised $(Ce/Yb)_N$, Ce and $(Dy/Yb)_N$ showing that Rare Earth Element Ratios (REE) can best be explained by extensive fractional crystallization of clinopyroxene also observed in the petrography of the Epi lavas. Partition coefficients used are those from Fujimaki et al. (1984).

Supplemental Fig. S2. a) CaO/Al_2O_3 versus SiO_2, b) Dy/Dy* versus SiO_2 and c) Dy/Dy* versus chondrite normalised $(Dy/Yb)_N$. Dy/Dy* calculated as in Davidson et al. (2012). Extensive fractionation model similar to that used in Supplemental Fig. S1. Chondrite normalised values from Sun and McDonough (1989).

Tectonic control on the genesis of magmas in the New Hebrides arc (Vanuatu)

Christoph Beier[1], Philipp A. Brandl[2], Selma M. Lima[1] and Karsten M. Haase[1]

[1]GeoZentrum Nordbayern, Friedrich-Alexander Universität Erlangen-Nürnberg, Schlossgarten 5, D-91054 Erlangen, Germany, Email: christoph.beier@fau.de

[2]GEOMAR Helmholtz-Zentrum für Ozeanforschung Kiel, Wischhofstraße 1-3, 24148 Kiel, Germany

Table 1. Representative whole rock and glass major element, trace element and Sr-Nd-Pb isotope data. Full dataset for glasses, glass inclusions and minerals available in supplemental Tables 1 and 3. Methods as described in the main text. Whole rock major element analyses performed by XRF, trace element analyses of glasses and whole rock samples by solution ICP-MS at the GeoZentrum Nordbayern, Friedrich-Alexander Universität Erlangen-Nürnberg following methods also described in Lima et al. (2017). Major elements of the glasses were determined using an electron microprobe. International Geo Sample Numbers (IGSN) registered at System for Earth Sample Registration (SESAR, http://geosamples.org). Errors for spiked Pb analyses are generally ±0.002, ±0.0019 and ±0.0046 for 206Pb/204Pb, 207Pb/204Pb and 208Pb/204Pb, respectively.

Cruise	R/V Sonne 229 Corioli s Throug hs	R/V Sonne 229 Corioli s Throug hs	R/V Sonne 229 Corioli s Throug hs	R/V Sonne 229 Corioli s Throug hs	R/V Sonne 229 Corioli s Throug hs	R/V Sonne 229 Corioli s Throug hs	R/V Sonne 229 Corioli s Throug hs	R/V Sonne 229 Corioli s Throug hs	R/V Sonne 229 Corioli s Throug hs	R/V Sonne 229 Corioli s Throug hs	R/V Sonne 229 Corioli s Throug hs	R/V Sonne 229 Corioli s Throug hs	R/V Sonne 229 Corioli s Throug hs	R/V Sonne 229 Corioli s Throug hs	R/V Sonne 229 Corioli s Throug hs	R/V Sonne 229 Corioli s Throug hs
Sample ID	008-TVG-01g	017-TVG-01	017-TVG-02	017-TVG-06	026-TVG-01	026-TVG-02	026-TVG-05	026-TVG-06	006-ROV-01	006-ROV-11	006-ROV-13	009-TVG-01a	009-TVG-01c	013-ROV-10	016-TVG-03	024-TVG-01	025-TVG-02
IGSN	IEGZN 0550	IEGZN 0561	IEGZN 0562	IEGZN 0563	IEGZN 0567	IEGZN 0568	IEGZN 0569	IEGZN 0570	IEGZN 0542	IEGZN 0548	IEGZN 0549	IEGZN 0551	IEGZN 0553	IEGZN 0559	IEGZN 0560	IEGZN 0564	IEGZN 0566
Locality	EPI B/Cioan	EPI G	EPI G	EPI G	EPI C	EPI C	EPI C	EPI C	EPi C/G	EPi C/G	EPi C/G	EPI F	EPI F	EPI D	EPI E	EPI B/Cioan/C	EPI B/Cioan/C
Lat. S (dec)	16.6900	16.7210	16.7210	16.7210	16.6990	16.6990	16.6990	16.6990	16.7000	16.6900	16.6900	16.6980	16.6980	16.6890	16.6990	16.6870	16.6900
Long. E (dec)	168.3840	168.3870	168.3870	168.3870	168.4270	168.4270	168.4270	168.4270	168.4100	168.4100	168.4100	168.3950	168.3950	168.4100	168.3820	168.4080	168.4100
Depth (m)	-182	-349	-349	-349	-225	-225	-225	-225	-362	-333	-334	-220	-220	-307	-243	-331	-329

Material	WR	WR	WR	WR	WR	WR	WR	WR	GL	GL	GL	GL	GL	GL	GL	GL	GL
[wt.%]																	
SiO2 SiO2	61.60	49.00	48.40	60.70	50.30	46.10	48.80	49.00	70.37	67.37	66.30	66.40	68.20	69.00	69.10	58.40	68.70
TiO2TiO2	0.62	0.59	0.56	0.61	0.53	0.94	0.49	0.64	0.41	0.51	0.42	0.49	0.39	0.44	0.47	0.61	0.49
Al2O3Al2O3	14.96	16.72	17.57	15.14	16.83	14.81	17.73	17.20	14.12	14.55	13.77	15.07	14.69	14.42	14.18	15.82	14.32
FeO									3.66	4.61	3.72	4.82	4.08	3.95	3.80	7.95	4.14
Fe2O3Fe2O3	7.05	10.10	10.00	7.00	9.68	15.94	9.40	10.80									
MnO	0.15	0.16	0.15	0.15	0.17	0.21	0.15	0.17	0.05	0.14	0.13	0.12	0.10	0.10	0.11	0.18	0.12
MgO	2.79	6.34	6.21	2.35	6.97	6.47	7.49	5.94	0.54	0.92	0.53	1.11	0.78	0.67	0.61	3.04	0.74
CaO	5.29	13.61	14.45	5.14	11.93	12.62	12.92	12.75	1.87	2.87	1.86	3.30	2.54	2.20	2.02	6.78	2.22
Na2ONa2O	3.79	2.24	1.88	4.14	2.25	2.06	1.96	2.35	3.80	3.75	3.77	3.72	3.68	3.82	3.65	3.27	3.75
K2OK2O	3.32	0.87	0.40	3.15	1.01	0.52	0.72	0.83	4.71	4.34	4.67	4.08	4.39	4.59	4.57	2.67	4.53
P2O5P2O5	0.25	0.09	0.11	0.23	0.11	0.10	0.09	0.13	0.10	0.10	0.11	0.09	0.10	0.12	0.11	0.16	0.12
Cl									0.26	0.27	0.34	0.25	0.28	0.28	0.31	0.18	0.28
SO3SO3									0.01	0.01	0.03	0.01	0.03	0.02	0.05	0.04	0.02
LOI	0.02	0.11	0.12	1.19	0.01	0.29	0.03	0.07									
Total	99.84	99.83	99.85	99.80	99.79	100.06	99.77	99.88	99.83	99.39	95.56	99.43	99.19	99.56	98.88	99.09	99.35
[ppm]																	
Li	12.4	6.09	4.49	12.6	6.87	4.74	5.61	7.08	21.9	16.5	19.7	17.7	18.9	19.7	22.0	13.8	17.8

Sc	20.1	42.5	48.1	16.4	36.6	49.2	37.2	38.9	8.49	9.07	7.67	12.8	12.1	9.40	9.76	30.8	15.1
V	120	293	315	124	253	724	248	332	28.9	44.4	29.0	73.7	70.1	41.2	52.0	288	101
Cr	28.7	41.7	44.6	10.0	112	4.26	116	63.9	2.94	1.69	50.3	10.9	9.61	4.37	8.25	60.0	1.90
Co	16.5	31.7	32.6	16.0	36.5	47.3	35.5	32.1	5.34	6.68	5.86	10.3	10.2	6.86	7.18	26.0	13.2
Ni	14.0	27.9	27.0	9.16	50.3	27.3	54.9	37.1	2.27	6.36	30.2	6.47	6.28	2.63	4.00	20.0	5.30
Cu	44.3	73.8	63.1	47.7	87.0	105	87.1	72.3	38.3	39.1	60.9	40.5	50.2	39.0	56.3	115	56.4
Zn	80.1	59.1	57.4	83.1	70.3	77.5	53.7	62.8	74.5	63.7	79.0	77.4	87.0	82.7	64.4	67.0	106
Ga	25.2	14.0	16.4	15.9	16.4	18.4	15.8	14.5	37.7	30.7	34.7	34.0	30.8	32.1	43.4	36.1	35.2
Rb	64.6	14.8	6.50	59.5	18.7	8.83	12.8	14.2	81.4	60.3	75.4	67.3	70.1	81.5	109	55.2	66.0
Sr	298	423	476	299	473	527	490	530	146	163	220	205	214	161	206	419	285
Y	28.3	12.9	11.1	28.9	13.0	12.3	10.7	13.3	28.6	22.2	24.6	25.4	24.7	31.2	22.6	18.0	29.6
Zr	157	47.3	23.8	175	54.0	28.5	36.7	41.8	211	156	213	217	208	230	222	131	190
Nb	4.05	0.981	0.487	3.72	1.20	0.572	0.860	0.836	5.02	3.73	4.90	4.75	4.46	5.13	4.79	2.78	4.19
Mo	2.13	0.666	0.387	2.26	1.20	0.778	0.630	0.775	4.99	3.66	4.32	3.47	3.53	2.82	3.62	2.21	8.78
Cs	1.21	n.d.	n.d.	n.d.	0.601	0.306	n.d.	n.d.	4.05	3.01	2.10	2.06	1.93	2.07	2.60	1.55	3.48
Ba	555	137	81.8	500	184	105	129	155	594	465	660	623	600	652	891	572	530
La	18.1	4.86	2.97	17.9	6.03	3.63	4.51	5.24	19.4	15.1	19.2	19.1	18.4	21.9	18.8	12.7	18.6
Ce	40.4	10.6	6.88	37.9	13.4	8.52	9.82	11.5	41.8	32.2	42.7	45.1	40.7	47.9	57.0	30.9	38.6
Pr	5.22	1.53	1.09	4.98	1.85	1.29	1.41	1.69	5.33	4.14	5.38	5.31	5.21	6.06	5.89	3.92	5.12
Nd	22.0	7.26	5.59	21.4	8.28	6.30	6.54	8.08	21.4	16.8	21.5	21.4	21.1	24.6	23.0	16.2	21.5
Sm	5.13	2.04	1.74	5.13	2.19	1.93	1.79	2.28	4.65	3.65	4.58	4.67	4.58	5.40	4.95	3.73	4.77
Eu	1.17	0.636	0.621	1.16	0.669	0.685	0.552	0.724	0.845	0.746	1.05	0.951	0.977	1.03	1.04	0.975	1.04
Gd	4.88	2.18	1.94	4.83	n.d.	n.d.	1.84	2.36	4.30	3.41	4.44	4.67	4.57	5.08	n.d.	n.d.	4.70
Tb	0.721	0.355	0.317	0.761	0.354	0.346	0.295	0.376	0.650	0.512	0.645	0.674	0.650	0.779	0.657	0.540	0.710
Dy	4.56	2.27	2.02	4.78	2.27	2.23	1.88	2.38	4.22	3.33	4.11	4.28	4.17	4.94	4.19	3.44	4.57
Ho	0.920	0.460	0.406	0.974	0.458	0.452	0.382	0.479	0.890	0.695	0.865	0.896	0.865	1.04	0.873	0.717	0.953

Er	2.73	1.33	1.16	2.90	1.34	1.28	1.11	1.37	2.74	2.13	2.63	2.73	2.64	3.17	2.63	2.12	2.89
Tm	0.410	0.193	0.164	0.433	0.195	0.181	0.160	0.198	0.425	0.323	0.401	0.412	0.397	0.491	0.408	0.321	0.444
Yb	2.78	1.28	1.08	2.94	1.31	1.19	1.07	1.30	2.95	2.29	2.87	2.94	2.83	3.39	2.90	2.22	2.99
Lu	0.429	0.195	0.162	0.460	0.198	0.179	0.163	0.196	0.457	0.352	0.432	0.441	0.421	0.529	0.430	0.331	0.476
Hf	4.10	1.39	0.781	4.81	1.52	0.910	1.10	1.28	4.90	3.68	5.61	5.49	5.40	6.09	4.99	2.93	4.71
Ta	0.213	0.059	0.029	0.228	0.072	0.039	0.049	0.051	0.228	0.165	0.298	0.278	0.262	0.295	0.239	0.136	0.202
W	0.316	0.116	0.064	0.444	0.161	0.085	0.099	0.106	0.535	0.382	0.806	0.539	0.522	0.570	0.594	0.369	0.432
Pb	9.27	3.30	2.09	11.5	3.77	2.24	5.14	3.68	9.62	7.60	12.5	12.8	12.0	12.1	13.3	8.33	8.49
Th	3.56	0.859	0.348	3.63	1.13	0.517	0.807	0.868	4.40	3.36	4.62	4.36	4.29	5.19	4.64	2.92	3.89
U	1.48	0.346	0.183	1.22	0.421	0.197	0.317	0.328	1.65	1.25	1.78	1.64	1.68	1.80	2.27	1.32	3.73
87Sr/86Sr	0.704214±7	0.704204±7	0.704214±6	0.704197±6	0.70422±7	0.704232±6	0.704227±8	0.704197±7									
143Nd/144Nd		0.512948±4	0.512954±4	0.512938±4		0.512938±4	0.512943±4	0.512943±4									
206Pb/204Pb	18.486	18.504	18.503	18.485	18.464	18.487	18.406	18.500									
207Pb/204Pb	15.552	15.551	15.542	15.549	15.513	15.539	15.548	15.554									
208Pb/204Pb	38.457	38.452	38.425	38.448	38.329	38.416	38.339	38.459									

HIGHLIGHTS

- Epi melts have experienced no disequilibrium modification by mixing or assimilation
- Melts fractionate continuously while ascending, rather than stagnating
- Magma ascent is through a complex system of dykes and sills
- Epi situated between compressional and extensional regime on thick island arc crust
- Structural features have impact on focusing and composition of island arc magmas

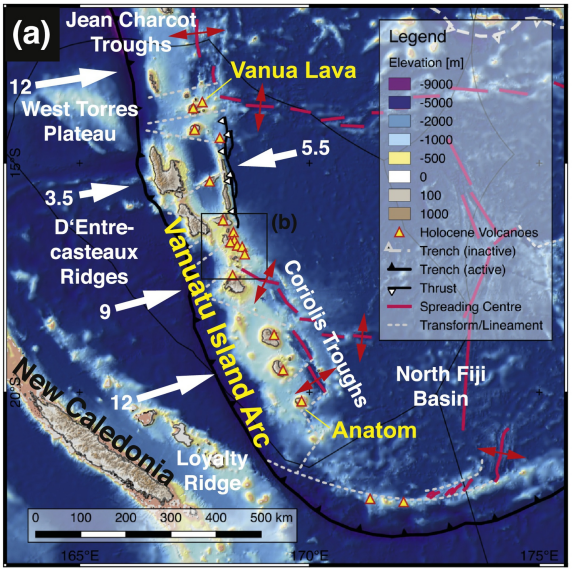
(a)
Jean Charcot Troughs
Vanua Lava
12
West Torres Plateau
5.5
3.5
D'Entre-casteaux Ridges
(b)
Vanuatu Island Arc
Coriolis Troughs
9
12
North Fiji Basin
New Caledonia
Anatom
Loyalty Ridge
Legend
Elevation [m]
-9000
-5000
-2000
-1000
-500
0
100
1000
Holocene Volcanoes
Trench (inactive)
Trench (active)
Thrust
Spreading Centre
Transform/Lineament
0 100 200 300 400 500 km
165°E
170°E
175°E

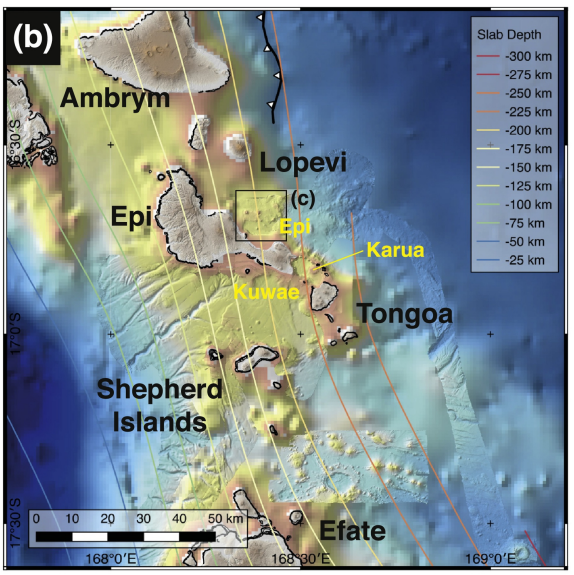
(b)
Ambrym
Lopevi
Epi
(c)
Epi
Karua
Kuwae
Tongoa
Shepherd Islands
Efate
Slab Depth
-300 km
-275 km
-250 km
-225 km
-200 km
-175 km
-150 km
-125 km
-100 km
-75 km
-50 km
-25 km
0 10 20 30 40 50 km
168°0'E
168°30'E
169°0'E

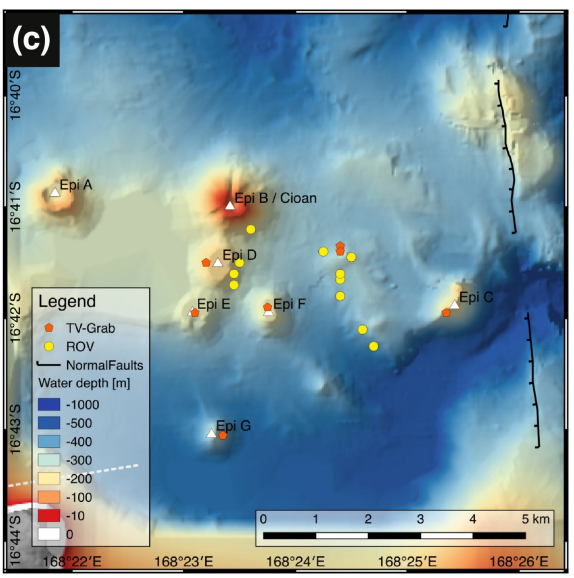
(c)
Epi A
Epi B / Cioan
Epi D
Epi E
Epi F
Epi C
Epi G
Legend
TV-Grab
ROV
NormalFaults
Water depth [m]
-1000
-500
-400
-300
-200
-100
-10
0
0 1 2 3 4 5 km
168°22'E
168°23'E
168°24'E
168°25'E
168°26'E

Figure 1

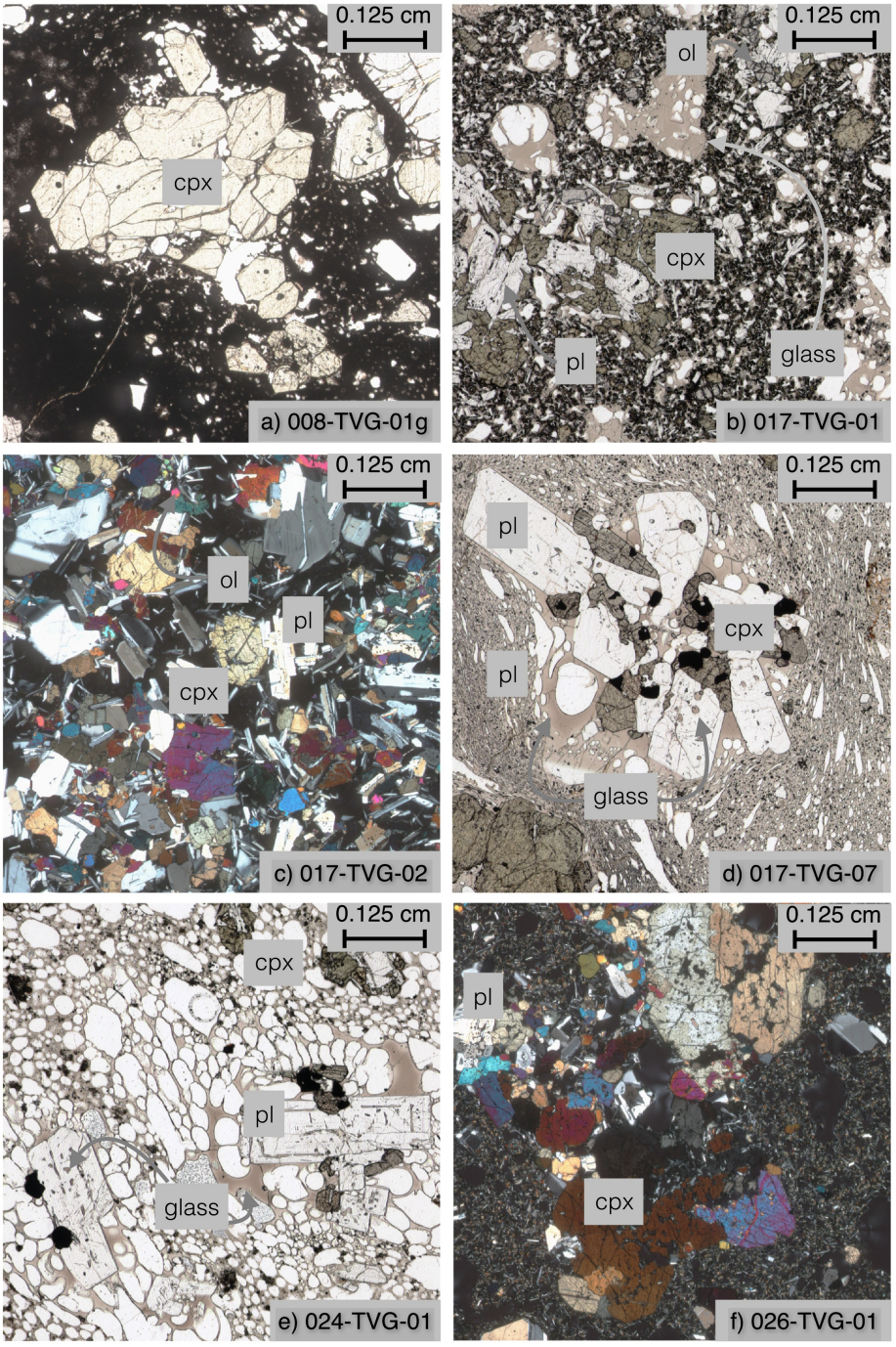
0.125 cm
cpx
a) 008-TVG-01g
0.125 cm
ol
cpx
pl
glass
b) 017-TVG-01
0.125 cm
ol
pl
cpx
c) 017-TVG-02
0.125 cm
pl
cpx
pl
glass
d) 017-TVG-07
0.125 cm
cpx
pl
glass
e) 024-TVG-01
0.125 cm
pl
cpx
f) 026-TVG-01

Figure 2

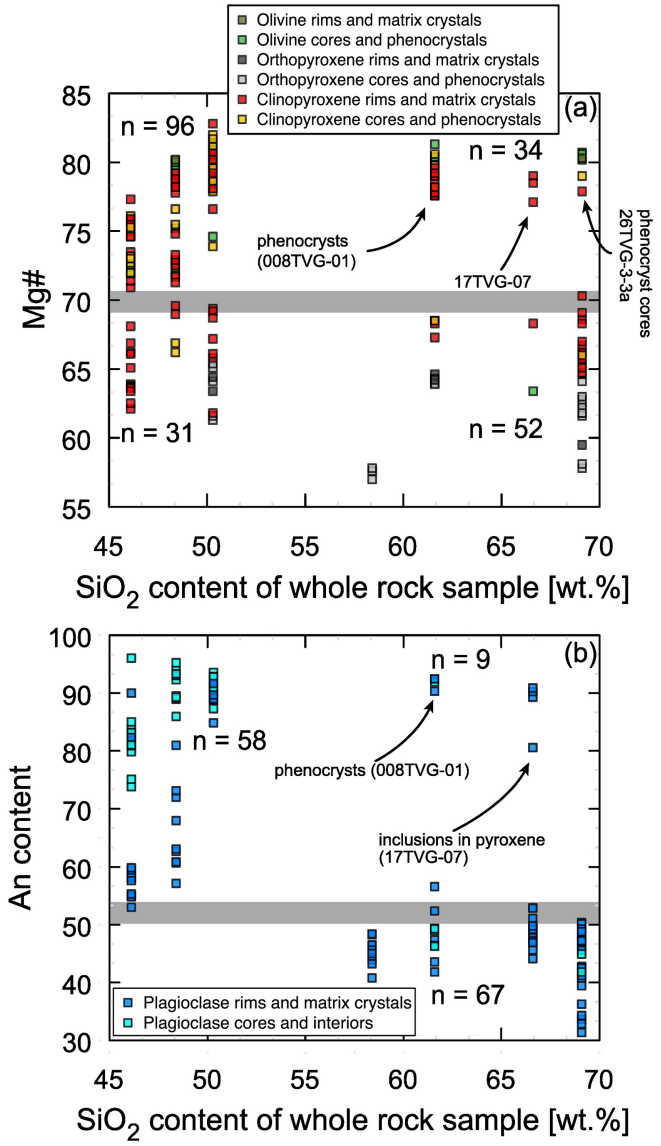
Olivine rims and matrix crystals
Olivine cores and phenocrystals
Orthopyroxene rims and matrix crystals
Orthopyroxene cores and phenocrystals
Clinopyroxene rims and matrix crystals
Clinopyroxene cores and phenocrystals
(a)
n = 96
n = 34
n = 31
n = 52
phenocrysts (008TVG-01)
17TVG-07
phenocryst cores 26TVG-3-3a
Mg#
SiO2 content of whole rock sample [wt.%]
(b)
n = 9
n = 58
n = 67
phenocrysts (008TVG-01)
inclusions in pyroxene (17TVG-07)
Plagioclase rims and matrix crystals
Plagioclase cores and interiors
An content
SiO2 content of whole rock sample [wt.%]

Figure 3

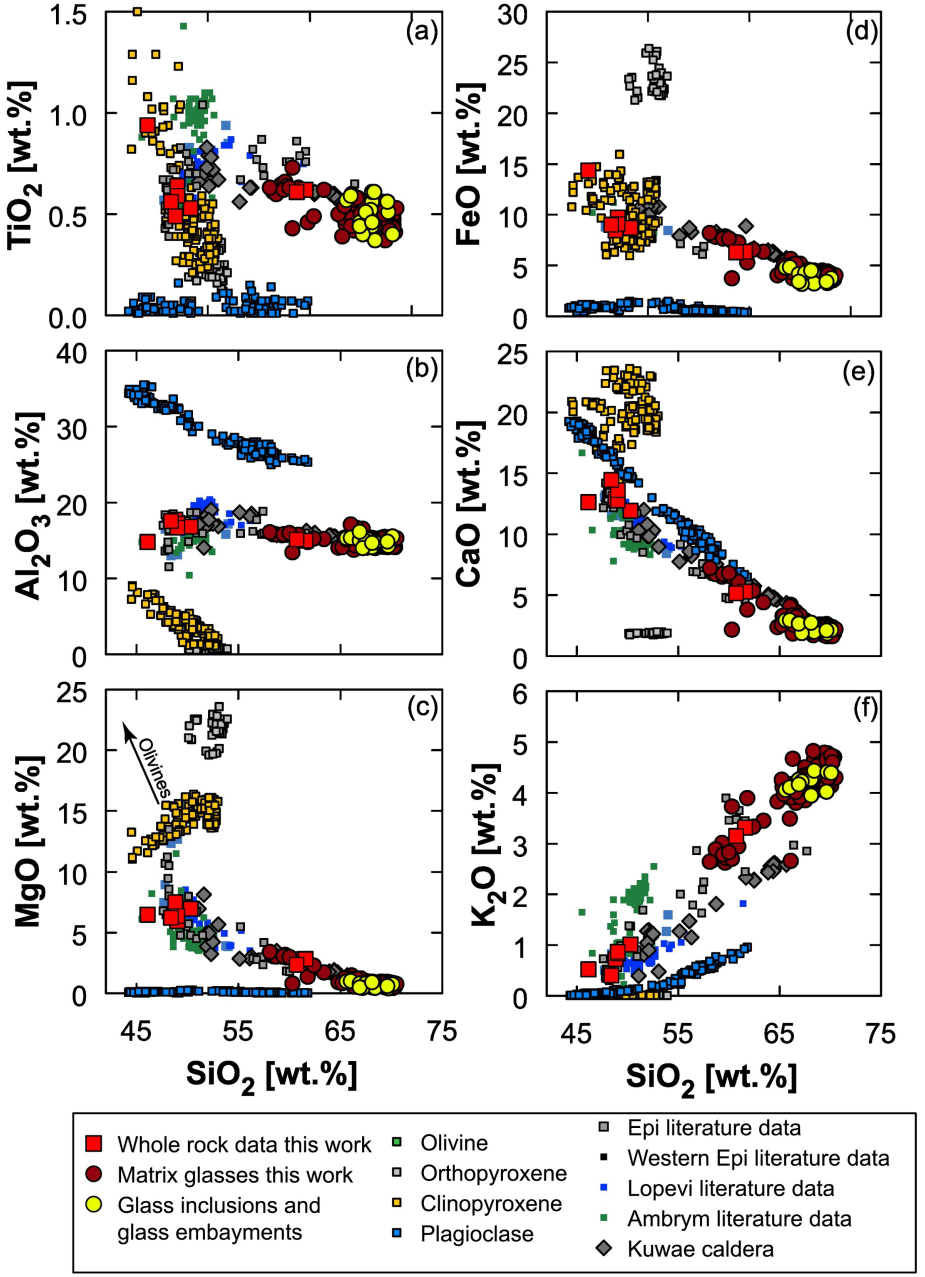
(a)
(b)
(c)
(d)
(e)
(f)
TiO2 [wt.%]
Al2O3 [wt.%]
MgO [wt.%]
FeO [wt.%]
CaO [wt.%]
K2O [wt.%]
SiO2 [wt.%]
SiO2 [wt.%]
Olivines
Whole rock data this work
Matrix glasses this work
Glass inclusions and glass embayments
Olivine
Orthopyroxene
Clinopyroxene
Plagioclase
Epi literature data
Western Epi literature data
Lopevi literature data
Ambrym literature data
Kuwae caldera

Figure 4af

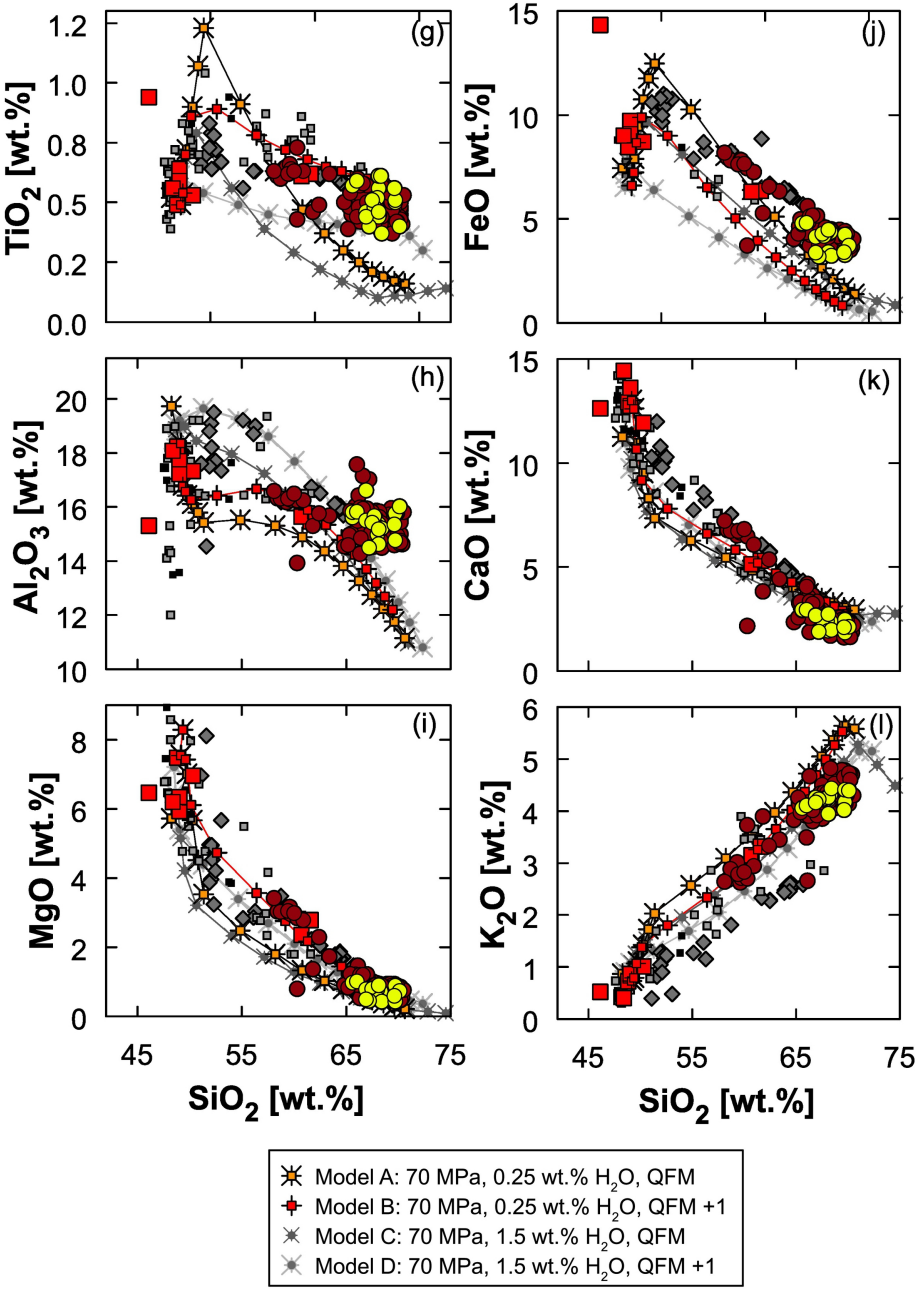
(g)
TiO2 [wt.%]
(j)
FeO [wt.%]
(h)
Al2O3 [wt.%]
(k)
CaO [wt.%]
(i)
MgO [wt.%]
(l)
K2O [wt.%]
SiO2 [wt.%]
SiO2 [wt.%]
Model A: 70 MPa, 0.25 wt.% H2O, QFM
Model B: 70 MPa, 0.25 wt.% H2O, QFM +1
Model C: 70 MPa, 1.5 wt.% H2O, QFM
Model D: 70 MPa, 1.5 wt.% H2O, QFM +1

Figure 4gl

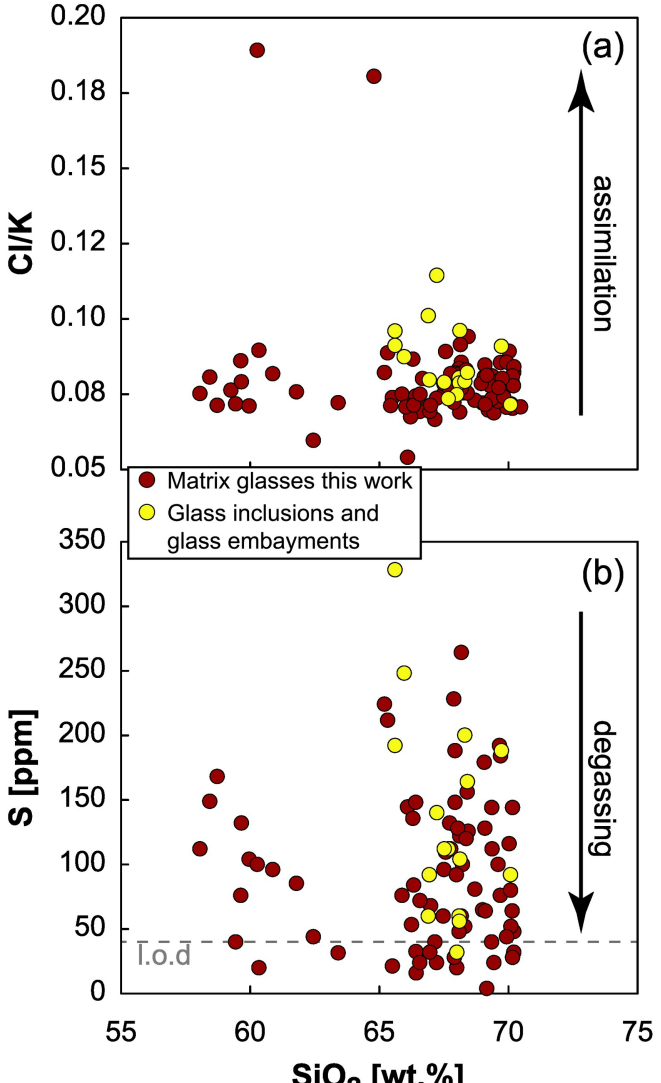
(a)
Cl/K
0.20
0.18
0.15
0.12
0.10
0.08
0.05
assimilation
Matrix glasses this work
Glass inclusions and glass embayments
(b)
S [ppm]
350
300
250
200
150
100
50
0
l.o.d
degassing
55
60
65
70
75
SiO2 [wt.%]

Figure 5

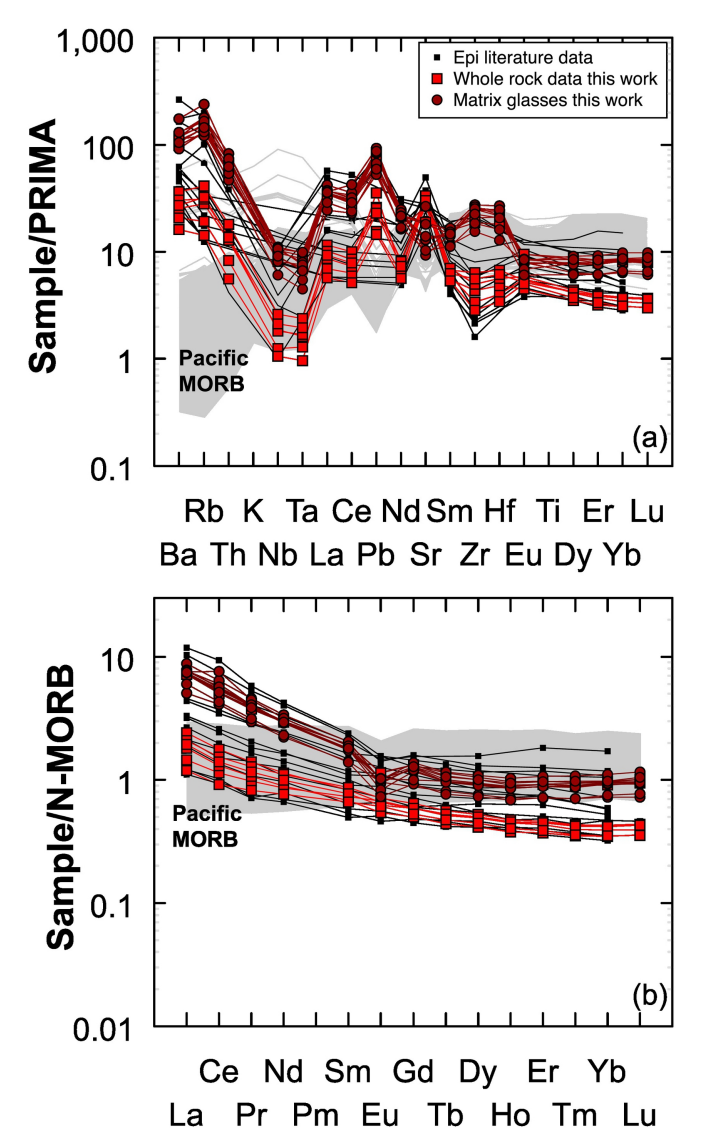
Epi literature data
Whole rock data this work
Matrix glasses this work
Sample/PRIMA
1,000
100
10
1
0.1
Pacific
MORB
(a)
Rb K Ta Ce Nd Sm Hf Ti Er Lu
Ba Th Nb La Pb Sr Zr Eu Dy Yb
Sample/N-MORB
10
1
0.1
0.01
Pacific
MORB
(b)
Ce Nd Sm Gd Dy Er Yb
La Pr Pm Eu Tb Ho Tm Lu

Figure 6

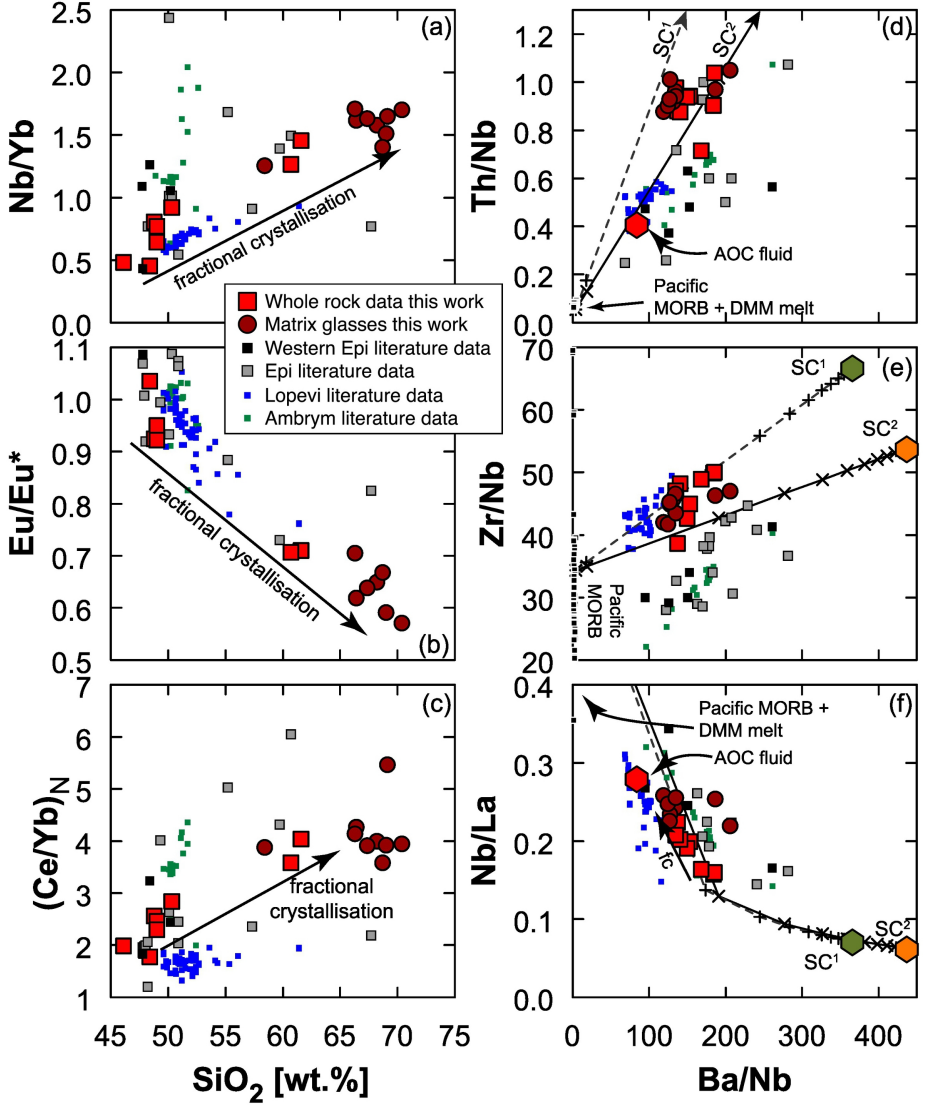
(a)
Nb/Yb
fractional crystallisation
(b)
Eu/Eu*
fractional crystallisation
(c)
(Ce/Yb)N
fractional crystallisation
SiO2 [wt.%]
Whole rock data this work
Matrix glasses this work
Western Epi literature data
Epi literature data
Lopevi literature data
Ambrym literature data
(d)
Th/Nb
SC1
SC2
AOC fluid
Pacific
MORB + DMM melt
(e)
Zr/Nb
SC1
SC2
Pacific
MORB
(f)
Nb/La
Pacific MORB +
DMM melt
AOC fluid
fc
SC2
SC1
Ba/Nb

Figure 7

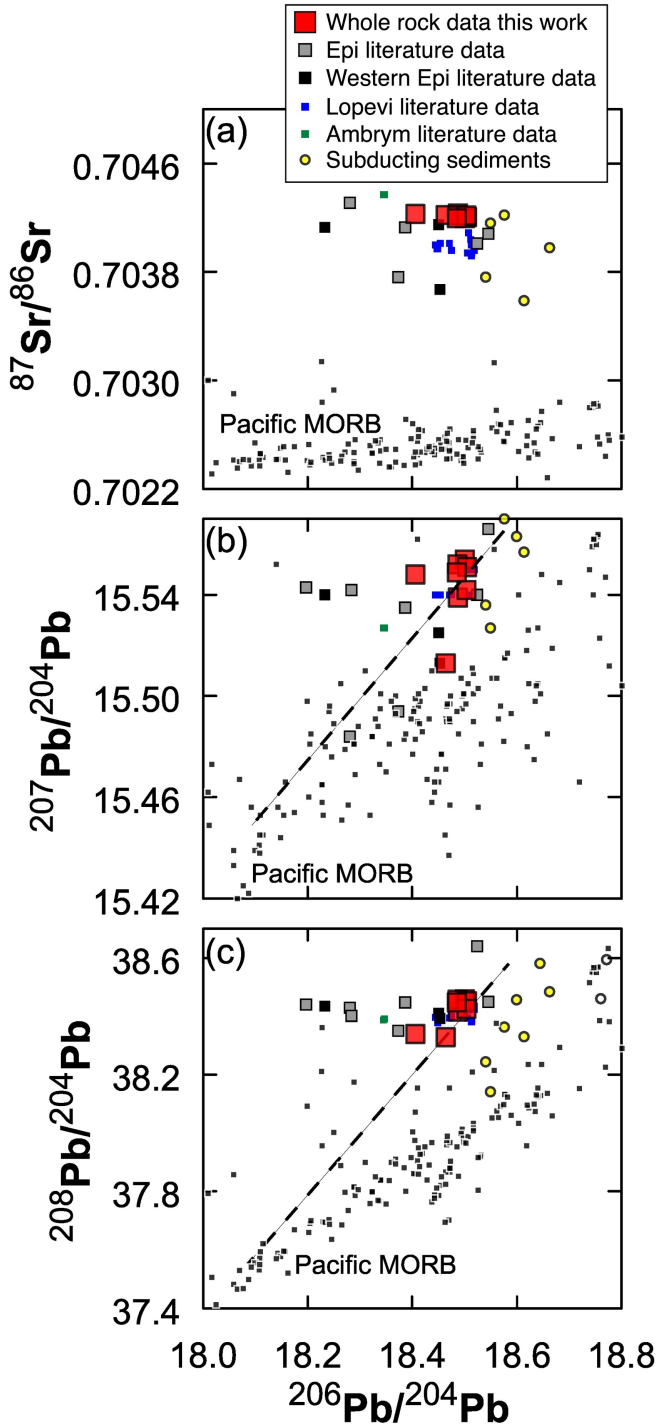
Whole rock data this work
Epi literature data
Western Epi literature data
Lopevi literature data
Ambrym literature data
Subducting sediments
(a)
0.7046
0.7038
0.7030
0.7022
$^{87}Sr/^{86}Sr$
Pacific MORB
(b)
15.54
15.50
15.46
15.42
$^{207}Pb/^{204}Pb$
Pacific MORB
(c)
38.6
38.2
37.8
37.4
$^{208}Pb/^{204}Pb$
Pacific MORB
18.0
18.2
18.4
18.6
18.8
$^{206}Pb/^{204}Pb$

Figure 8

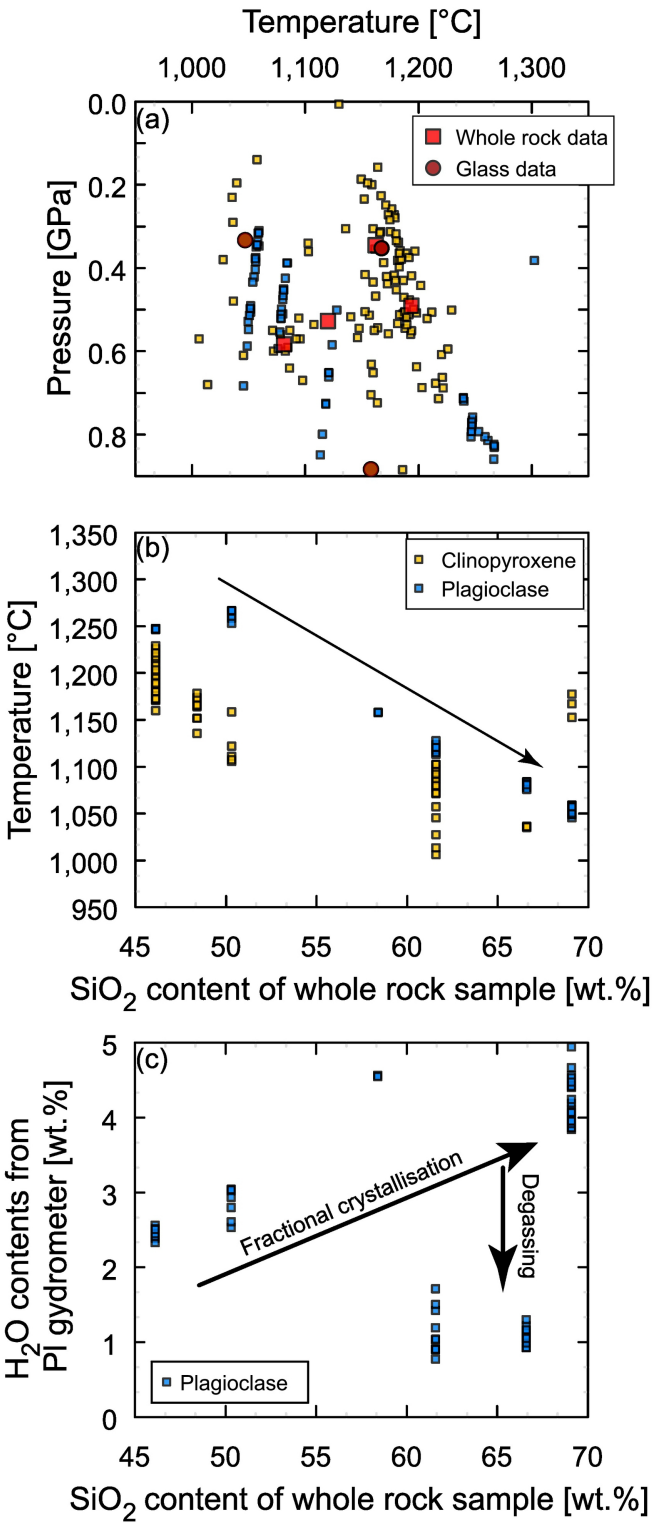
Temperature [°C]
1,000
1,100
1,200
1,300
(a)
Whole rock data
Glass data
Pressure [GPa]
0.0
0.2
0.4
0.6
0.8
(b)
Clinopyroxene
Plagioclase
Temperature [°C]
1,350
1,300
1,250
1,200
1,150
1,100
1,050
1,000
950
45
50
55
60
65
70
SiO2 content of whole rock sample [wt.%]
(c)
Fractional crystallisation
Degassing
Plagioclase
H2O contents from Pl gydrometer [wt.%]
5
4
3
2
1
0
45
50
55
60
65
70
SiO2 content of whole rock sample [wt.%]

Figure 9

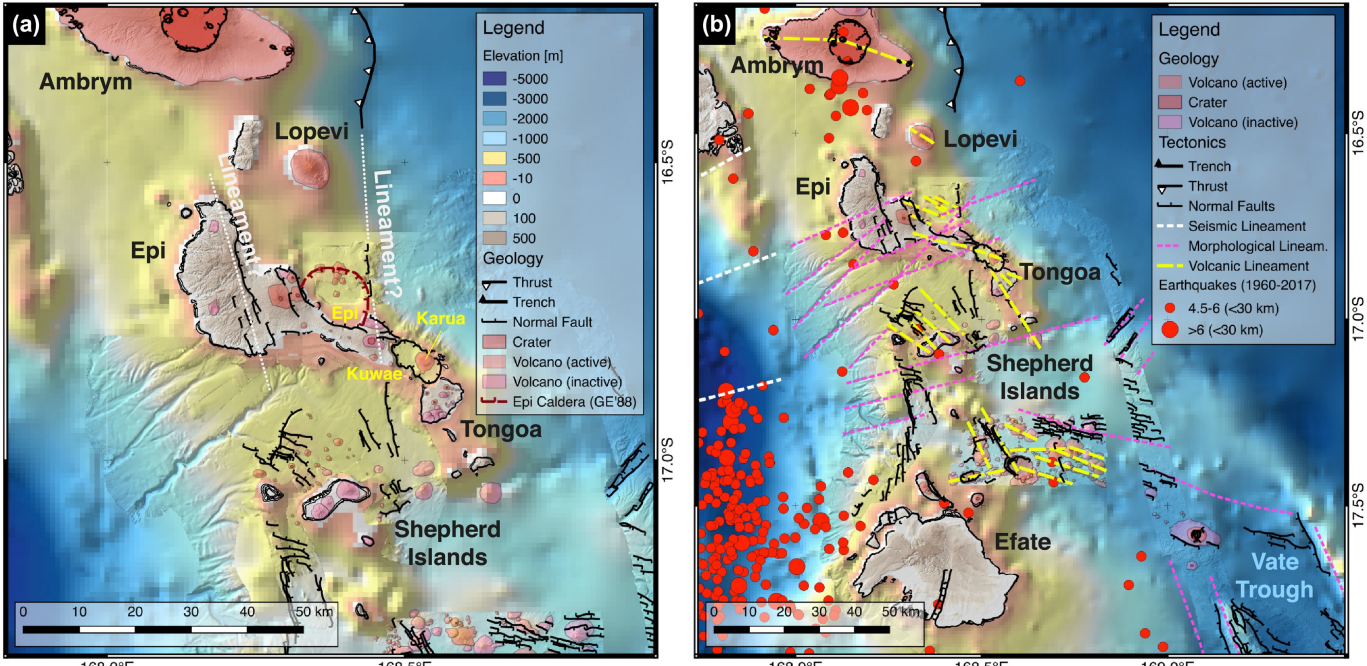
(a)
Ambrym
Lopevi
Epi
Lineament
Lineament?
Epi
Karua
Kuwae
Tongoa
Shepherd Islands
Legend
Elevation [m]
-5000
-3000
-2000
-1000
-500
-10
0
100
500
Geology
Thrust
Trench
Normal Fault
Crater
Volcano (active)
Volcano (inactive)
Epi Caldera (GE'88)
0 10 20 30 40 50 km
16.5°S
17.0°S
168.0°E
168.5°E
(b)
Ambrym
Lopevi
Epi
Tongoa
Shepherd Islands
Efate
Vate Trough
Legend
Geology
Volcano (active)
Crater
Volcano (inactive)
Tectonics
Trench
Thrust
Normal Faults
Seismic Lineament
Morphological Lineam.
Volcanic Lineament
Earthquakes (1960-2017)
4.5-6 (<30 km)
>6 (<30 km)
0 10 20 30 40 50 km
16.5°S
17.0°S
17.5°S
168.0°E
168.5°E
169.0°E

Figure 10

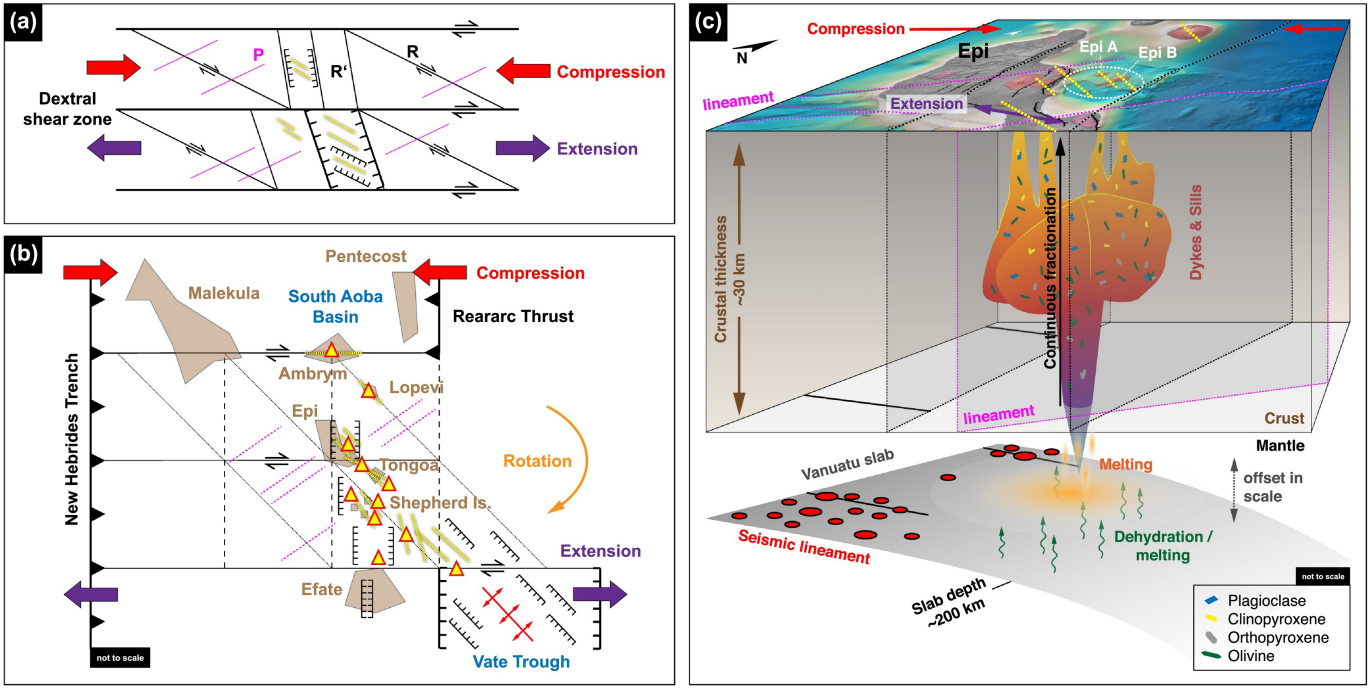
(a)
P
R
R'
Compression
Dextral
shear zone
Extension
(b)
Pentecost
Compression
Malekula
South Aoba
Basin
Rearare Thrust
Ambrym
Lopevi
Epi
Rotation
Tongoa
Shepherd Is.
New Hebrides Trench
Extension
Efate
not to scale
Vate Trough
(c)
Compression
N
Epi
Epi A
Epi B
lineament
Extension
Crustal thickness
~30 km
Continuous fractionation
Dykes & Sills
lineament
Crust
Mantle
Vanuatu slab
Melting
offset in
scale
Seismic lineament
Dehydration /
melting
Slab depth
~200 km
not to scale
Plagioclase
Clinopyroxene
Orthopyroxene
Olivine

Figure 11